

Article

Geologic Framework, Anthropogenic Impacts, and Hydrodynamics Contribute to Variable Sediment Availability and Shoreface Morphology at the Rockaway Peninsula, NY

Emily Wei *  and Jennifer Miselis

U.S. Geological Survey St. Petersburg Coastal and Marine Science Center, St. Petersburg, FL 33705, USA; jmiselis@usgs.gov

* Correspondence: ewei@usgs.gov

Abstract: Recent field and modeling studies have shown that barrier island resiliency is sensitive to sediment fluxes from the shoreface, making it important to evaluate how shoreface sediment availability varies in coastal systems. To do this, we assessed shoreface geology and morphology along the Rockaway Peninsula, NY, USA. We find that spatial variability in shoreface volume is influenced by sediment accommodation above the Holocene-Pleistocene (H-P) contact, historical barrier island evolution, and natural and engineered morphologic features, suggesting that simply identifying the H-P boundary may not be adequate for defining the shoreface reservoir. Further, sediment flux from the lower shoreface to the beach may be reduced by geologically limited cross-shore sediment distribution and shoreface steepening mediated by human modifications to the shoreline. Finally, the geologic limit of the shoreface is often shallower than a wave-based estimate of shoreface extent, implying that the geologic shoreface extent at our study site can be mobilized over short time scales (years-decades) and that the wave-based shoreface extent may be inaccurate when estimating shoreline response to sea-level rise. Our results demonstrate that the combination of hydrodynamics, humans, and geology on shoreface sediment fluxes impact how barrier islands respond to future changes in sediment supply and climate.

Keywords: coastal geomorphology; shorefaces; stratigraphy



Citation: Wei, E.; Miselis, J. Geologic Framework, Anthropogenic Impacts, and Hydrodynamics Contribute to Variable Sediment Availability and Shoreface Morphology at the Rockaway Peninsula, NY. *J. Mar. Sci. Eng.* **2022**, *10*, 989. <https://doi.org/10.3390/jmse10070989>

Academic Editors: Edward J. Anthony, Susana Costas and Duncan M. FitzGerald

Received: 16 May 2022

Accepted: 15 July 2022

Published: 20 July 2022

Publisher's Note: MDPI stays neutral with regard to jurisdictional claims in published maps and institutional affiliations.



Copyright: © 2022 by the authors. Licensee MDPI, Basel, Switzerland. This article is an open access article distributed under the terms and conditions of the Creative Commons Attribution (CC BY) license (<https://creativecommons.org/licenses/by/4.0/>).

1. Introduction

Recent studies have demonstrated that barrier islands and spits may not respond with uniformly transgressive behavior to sea-level rise and storms [1,2]. Instead, over timescales of years to centuries, barrier morphology and shoreline geometry may be affected by the sediment available in adjacent deposits, such as the shoreface and inner shelf [3–5]. The shoreface is a transitional zone located between the shoreline and continental shelf, the extent of which may be defined by the depth of transport, or the maximum depth at which morphological change occurs during extreme bed activity [6]. Shorefaces can either temporarily store sediment eroded from the beach or supply sediment to beaches through onshore transport by waves [7,8]. As such, slight changes in shoreface volumes could potentially redistribute large quantities of sand to the beach and barrier, thus affecting barrier resiliency to storms and increasing sea-level [7].

Moreover, predicting future coastal behavior often relies on measurements or parameterizations of coastal and shoreface morphology [9–11], wave climate and water levels [12], and the magnitude of sediment fluxes to and from the shoreface [13–16]. However, representative examples of shoreface morphology and sediment availability remain a critical knowledge gap [10]. In part, this is due to access issues; since the landward boundary of the shoreface is shallow and is where waves shoal and break, it is difficult to acquire bathymetric and geologic data there. Furthermore, a variety of processes operating over a wide spectrum of time scales can impact the volume and flux of erodible sediment from the

shoreface and inner shelf, such as antecedent topography [1,15,17–19], wave climate [11,20], and anthropogenic modifications to natural sediment budgets [21,22]. Therefore, to improve predictions of future coastal behavior, there is a need to characterize the morphology and geology of the shoreface and explore the relative influences of geologic framework, hydrodynamics, and anthropogenic alterations on shoreface sediment availability and distribution.

To that end, we acquired geophysical data from the shoreface along the Rockaway Peninsula, NY to quantify the volume of available sediment within the shoreface and understand how underlying geology influences shoreface sediment availability. Further, since the region has been almost continually altered by humans since the early 20th century, we explore the degree to which those changes have contributed to variability in shoreface sediment availability and distribution. The results herein build on previous work that emphasizes the importance of geologic processes in coastal evolution [8,17,19,23–31] and provide rare insight into the diverse nature of shoreface morphology and geology. This alongshore complexity in sediment availability may cause the barrier peninsula to respond to climate-driven changes in storminess and sea level in nonuniform ways.

2. Study Area

The study area is located in southwest Long Island, which was formed in association with two terminal moraines during the last glacial advance: the younger Harbor Hill and older Ronkonkoma [32]. To the north of Rockaway is the northeast-trending Harbor Hill moraine and to the south is glacial outwash (Figure 1) [33]. Erosion and reworking of glacial-derived sediment have contributed to much of the marine sediment offshore of Long Island, including Rockaway [34,35].

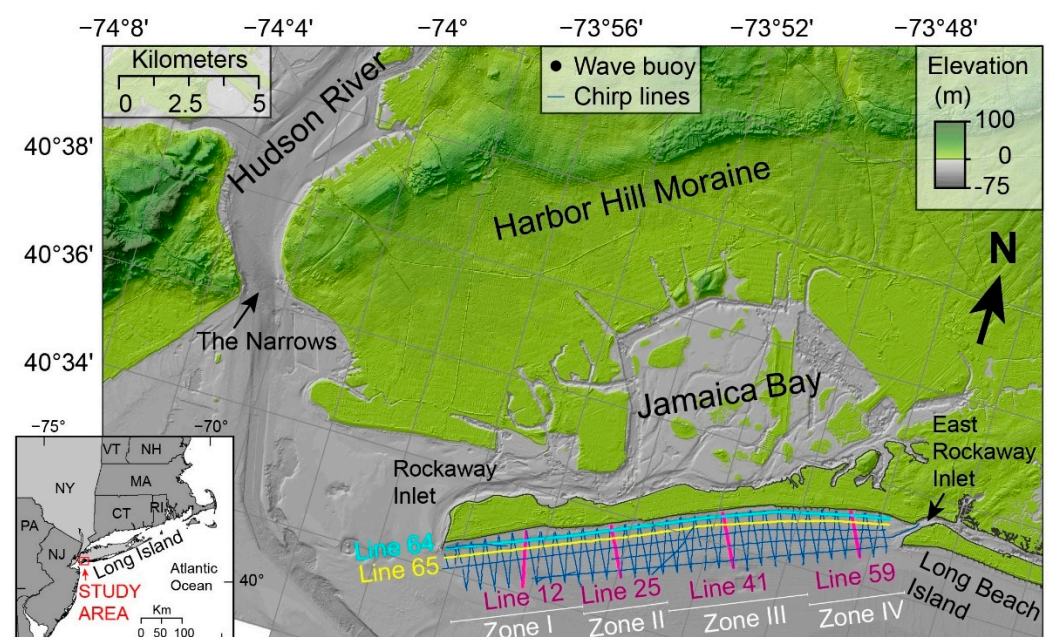


Figure 1. Location of the Rockaway, New York study area is indicated by the red rectangle in the bottom left inset. The geophysical survey spans the area from the nearshore to approximately two kilometers offshore of the Rockaway Peninsula. Chirp profiles acquired over the entire survey are shown in dark blue. In pink are dip lines shown in Figure 8, and strike lines highlighted in yellow and cyan are shown in Figures 9 and 10. The extents of geomorphic zones are indicated by the white lines on the barrier peninsula.

Offshore of Long Island, the thickness of sediment deposits is inconsistent from east to west, and controls on accommodation are likely exerted by the regional stratigraphic framework. The basal unit imaged in seismic profiles is the Upper Cretaceous-age coastal

plain strata that dips to the west [34], which may have influenced the location and course of the Hudson River during periods of lower sea-level [36,37]. Separating Cretaceous-age sediment from overlying deposits is a regional hiatus, over which Pleistocene sediment was deposited. Pleistocene sediment is composed of gravel to fine sand and is interpreted to be glaciofluvial outwash deposits that were deposited during Marine Isotope Stages (MIS) 2 and 4 [34,38,39]. At the outset of the Wisconsinian glaciation, Hudson Valley morphology was further modified by drainage of glacial lakes. Widespread evidence suggests that failure of the terminal moraine dam at the Narrows, to the west of Rockaway between Staten Island and Coney Island, resulted in widespread erosion of more than 100 m of Pleistocene and Cretaceous sediment [40] with redeposition of this material on the continental shelf [41].

Several thousand years following deglaciation, the net westward littoral drift formed the Rockaway Peninsula. It grew to its present length of 16 km over the past ~400 years [32,42]. Over the past 125 years, Rockaway peninsula has extended to the southwest by more than 6.4 km (Figure 2) [43]. This elongation rate was rapid until 1902, at which point rates decreased by 50% from 1902–1927 (Figure 2) [43,44]. For much of its existence, the Rockaway Peninsula has been occupied by humans. Prior to European settlement of Rockaway, Rockaway and Jamaica Bay served as the homelands of Indigenous people [44]. Beginning in 1914, European settlers and their descendants started to modify the peninsula [43]. On the western island terminus, a 2560 m long stone jetty was constructed in 1933 to stabilize the eastern side of Rockaway Inlet (Figure 1) [44]. Initial beach nourishment efforts were recorded as early as 1926 and subsequent beach renourishment projects between 1936–1965 occurred in response to large storm events (Figure 3) [45]. The combined efforts of jetty construction and beach renourishment halted westward elongation of the peninsula and forced it to prograde seaward, as evidenced by comparison of the 1934 and 1937 shorelines (Figure 2). The most extensive beach nourishment efforts began as part of the 1965 Flood Control Act in response to a severe storm in 1962 [44]. Estimates of beach renourishment are 3.8 million m³ between 1934–1961, 134,000 m³ between 1961–1973, and 14.3 million m³ between 1975–2019 (Figure 3) [44].

Over the long term (100-year trends), Rockaway has exhibited variable rates of erosion and accretion, with net accretion averaged over the peninsula due to beach renourishment (~0.5–1 m/yr) [45]. In the short term (20–30 years), there is erosion in east-central Rockaway and accretion in western Rockaway [44,46]. From a 32-year record of wave climate, average significant wave heights are approximately 0.96 m with an average dominant period of 8.20 seconds [47], but the region is exposed to greater wave energy during winter storms (nor'easters) and occasional hurricanes, such as Hurricane Sandy in 2012, which destroyed or caused substantial damage to 1,000 coastal structures [44]. The magnitude and direction of storm-waves has a significant impact on sediment dispersal and has moved sand emplaced on eastern beaches to western beaches [46] and likely contributes to the 344,000–459,000 m³ of sand that is estimated to move annually from east to west for parts of the south shore of Long Island [43]. Rockaway Beach is microtidal and tidal currents are generally weak; however, they increase in velocity at Rockaway Inlet and East Rockaway Inlet [44].

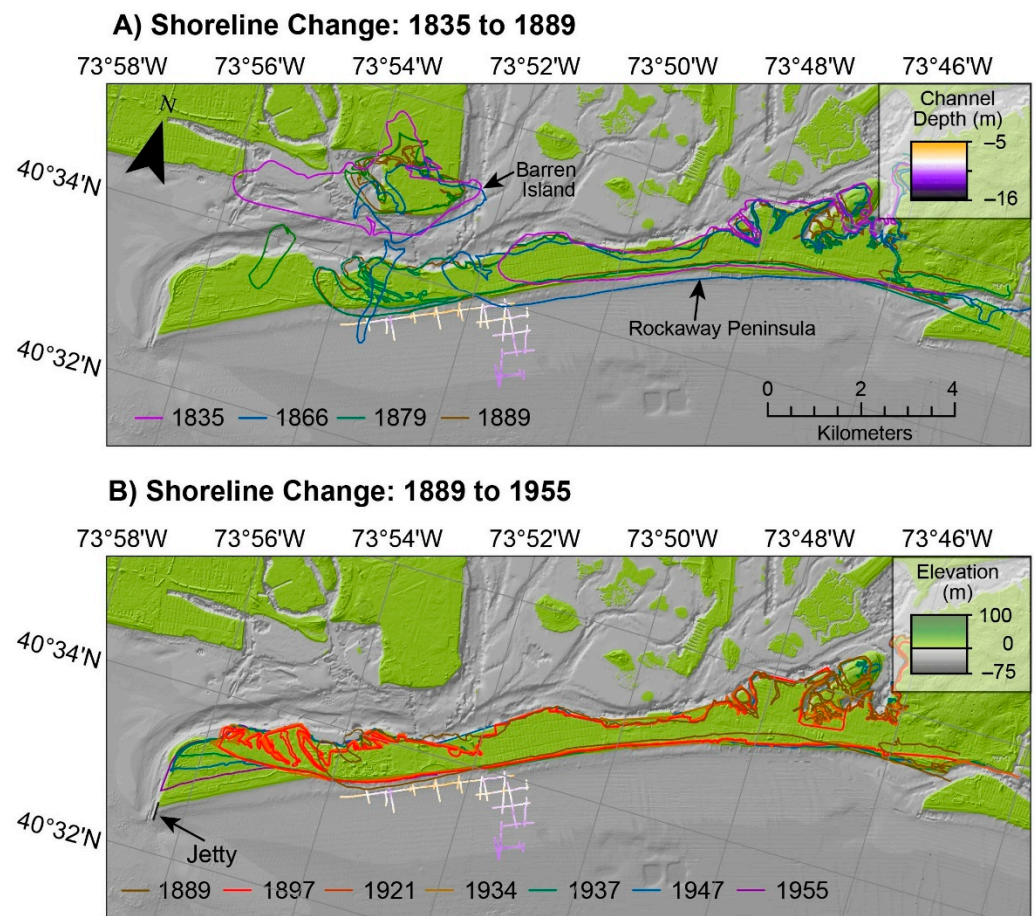


Figure 2. Rockaway shoreline evolution. Shorelines were digitized from maps from the NOAA Historical Map and Chart Collection (historicalcharts.noaa.gov). (A) Shoreline change of the Rockaway Peninsula from 1835–1889 was characterized by rapid westward progradation and growth. The shoreline of Barren Island, located northwest of the peninsula, is also shown through time. (B) The period from 1889–1995 is characterized by slow westward growth of the island until 1937, when the island elongated westward. Further growth from 1937–1955 is characterized by seaward progradation.

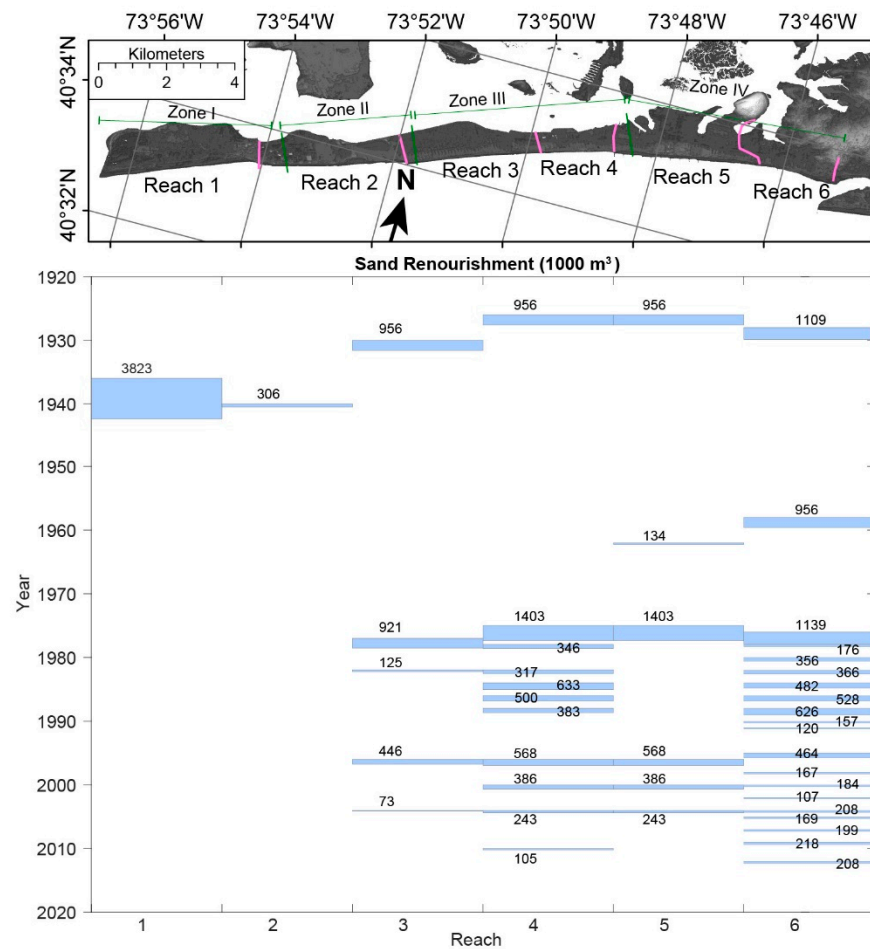


Figure 3. The volume and relative location of sand renourishment at the Rockaway Peninsula from 1920 through 2020. Blue bars indicate a renourishment event and are centered on the year during which they occurred. The widths of blue bars are proportional to their volume, which are labeled. Data for renourishment volumes are from U.S. Army Corps of Engineers (USACE) [46]. As the USACE data describe relative location by 6 reaches, the locations of these reaches are shown by pink vertical lines on the map. North of the peninsula, green bars and lines indicate the extent of geomorphic zones from this study.

3. Data Acquisition and Processing

In September–October 2019, the USGS acquired bathymetry and 201 km of Chirp seismic data in the nearshore region of the Rockaway Peninsula aboard the USGS Research Vessel (R/V) Sallenger, extending approximately 2 km offshore to the inner shelf and generally covering water depths < 20 m [48]. Shelf bathymetry was mapped using Teledyne Reson Seabat T50-P multibeam echosounders in dual-head configuration and a 200 kHz frequency. This resulted in 23.1 km² of bathymetry with 1 mm vertical resolution and 0.6 m pixel resolution [48] (Figure 4). More details on the acquisition and processing of multibeam data can be found in Stalk et al. [48]. Multibeam backscatter were also processed and exported as a raster for visualization in ArcMap (Figure 5).

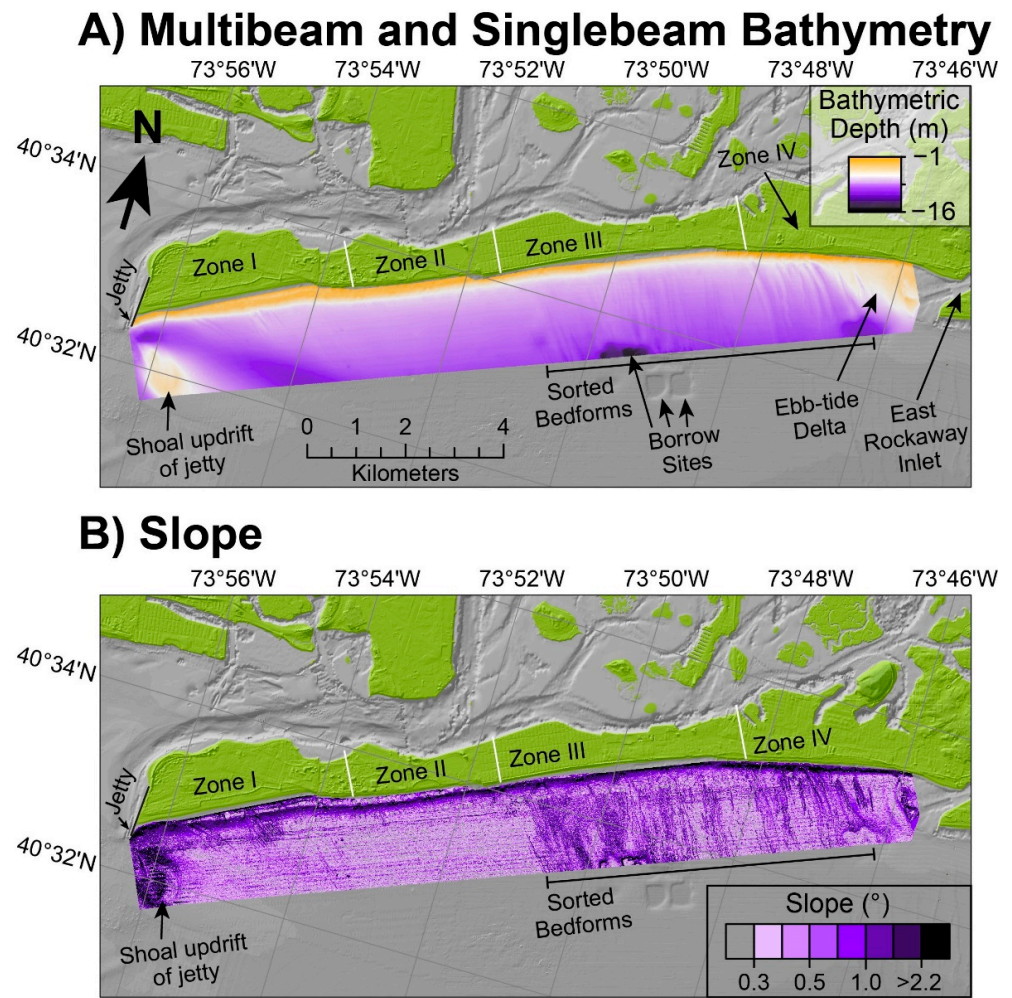


Figure 4. (A) Digital elevation model (DEM) of multibeam and single-beam bathymetry. (B) Slope of the DEM in degrees. Color scale for degrees is binned in quantiles. White lines on the peninsula delineate the boundaries of the geomorphic zones.

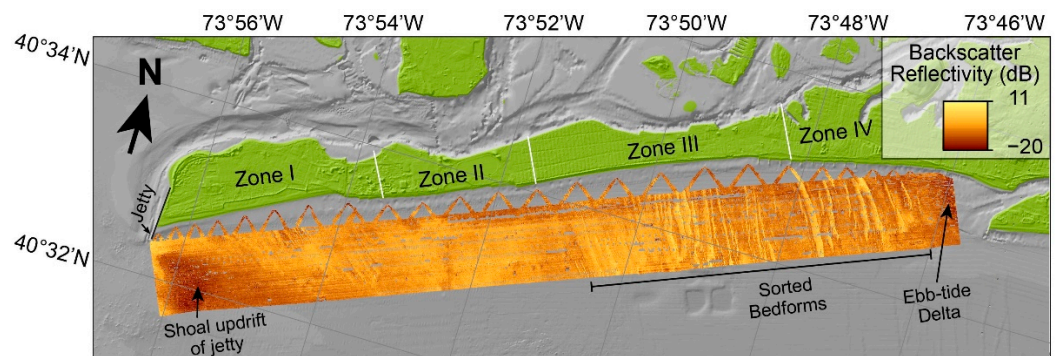


Figure 5. Multibeam backscatter. High reflectivity (bright colors) generally corresponds to harder seafloor substrate or increased roughness, whereas low reflectivity (dark colors) generally corresponds to softer substrate. White lines on the peninsula delineate the boundaries of the geomorphic zones.

Since multibeam swath bathymetry has a narrower footprint in shallow water and some shallow water areas were inaccessible to the vessel, 190 km of single-beam bathymetry was acquired in the surf zone (water depths ~0.5–9 m) using two Personal Watercraft (PWC) equipped with an Odom Echotrac CV100 single-beam sounder mounted to the stern [48]. Shore-perpendicular single-beam tracklines were spaced approximately 50 m

apart and were crossed by 2–3 shore-parallel tracklines. Additionally, a third single-beam echosounder was mounted on the frame in which the chirp seismic profiler was deployed (more details provided below). Data processing workflows for all single-beam datasets are described by Stalk et al. [48]. The overlapping coverage of the single-beam and multibeam surveys allowed for the creation of a seamless digital elevation model (DEM) using triangular irregular networks in ArcMap 10 (Figure 4) from which we extracted shore-perpendicular transects spaced at 50 m to assess shoreface morphology (Figure 6). Shoreface slopes were averaged within geomorphic zones and filtered in MATLAB (<https://www.mathworks.com/products/matlab.html>, accessed on 1 June 2022) using a lowpass infinite impulse response filter (Figure 6E).

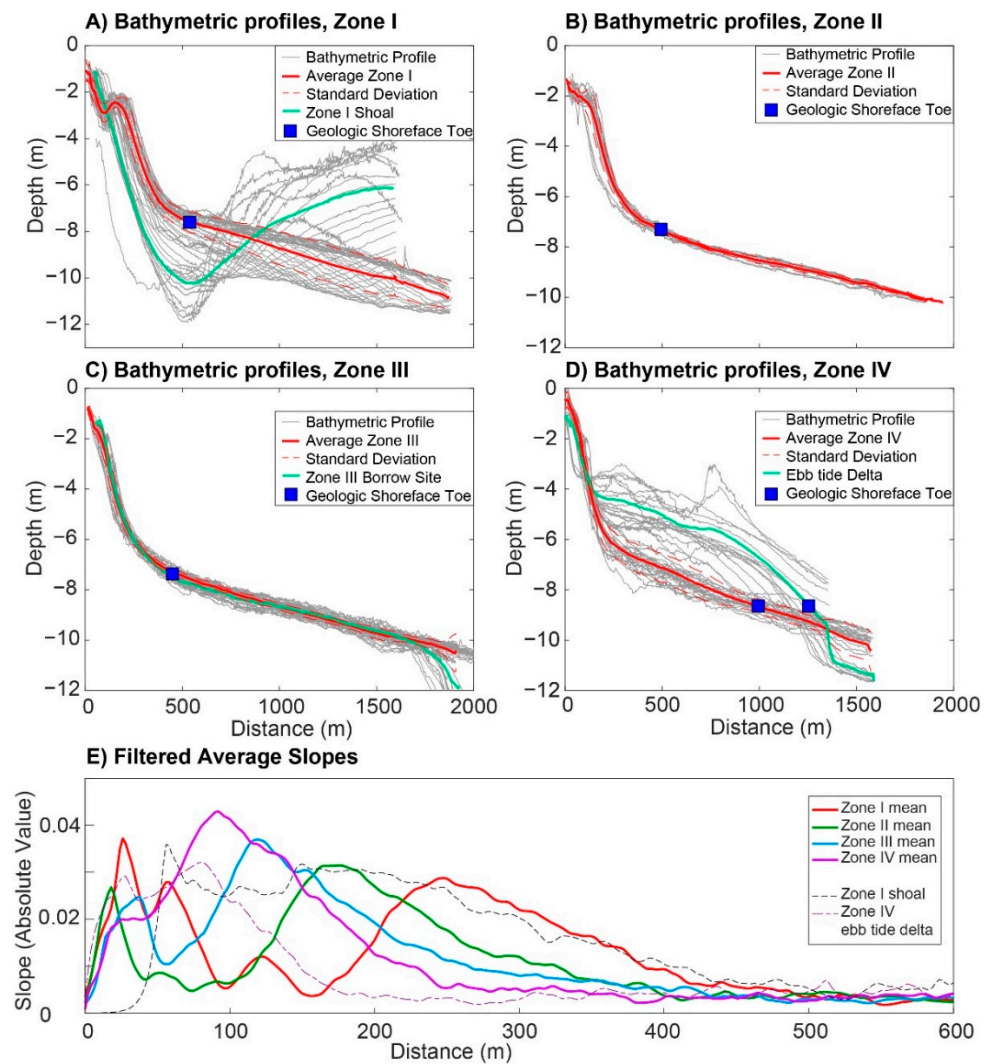


Figure 6. (A–D) Bathymetric profiles through the shoreface are shown for each geomorphic zone. Individual profiles are represented as gray lines; red lines represent the average; and green lines in (A,C,D) represent average bathymetry of geomorphic features. Blue squares on the profiles represent the average depth of the geologic shoreface toe (GST). (E) Slopes of each profile were averaged for zones I–IV, the zone I shoal, and the zone IV ebb tide delta. Filtered absolute values of average slope are shown.

Shoreface geological information was collected using an EdgeTech 512i subbottom profiler and an Ashtech Proflex 800 global positioning system (GPS) that were deployed in a purpose-built towed sled system. The seismic sled is buoyed by two inflatable pontoon floats that position the chirp just below the water’s surface and minimize the offset between the water surface and the chirp receiver. Furthermore, this setup allows for launching and

recovery of the seismic sled from shore. Chirp data were acquired at frequency ranges of 0.7–12 kHz, a pulse length of 20 milliseconds, and a ping rate of 5 Hz and were recorded in JSF and SEG-Y formats. Full waveform JSF files were enveloped and converted to SEG-Y files. More details on acquisition can be found in [49]. In Seismic Unix [50], the SEG-Y files were bandpass-filtered at frequencies of 3, 4, 10, and 12 kHz to remove shallow-water artifacts. Filtered SEG-Y files were imported into SonarWiz 7 (ChesapeakeTech.com, accessed on 5 May 2020) to apply heave corrections and time-varying gain. Then, the files were imported into the Kingdom software package (<https://ihsmarkit.com/products/kingdom-seismic-geological-interpretation-software.html>, accessed on 23 November 2021) for interpretation of surfaces. Interpretations of sediment units were based on sequence-stratigraphic principles [51,52]. The “math on two maps” tool in Kingdom Suite was used to calculate the difference (in two-way travel time) between the seafloor and interpreted surfaces. Two-way travel time was converted to sediment thickness using an internal sediment velocity of 1,650 m/s and a water column velocity of 1,500 m/s, following the methods used in a similar study at Fire Island, NY by Locker et al. [53]. Sediment unit thickness and reflector depth maps were gridded by using the surface function within Generic Mapping Tools software (version 5.4.5; <https://www.generic-mapping-tools.org>, accessed on 22 October 2020) and exported to Esri’s ArcMap geographic information system program for visualization.

A petite ponar deployed from the R/V Sallenger collected 32 surficial sediment grabs from the shoreface and inner shelf (Figure 7). Once the ponar sampling device recovered sediment and was on board, the sediment was subsampled and archived in zip-close bags, as described by Everhart et al. [54]. One terrestrial sample was recovered from scarped sediments under the boardwalk in eastern Rockaway (Figure 7). The surface layer was scraped off and a plastic container was used to collect the sample. Grain size analysis was conducted on a Coulter LS200 particle-size analyzer following the procedure described by Everhart et al. [54].

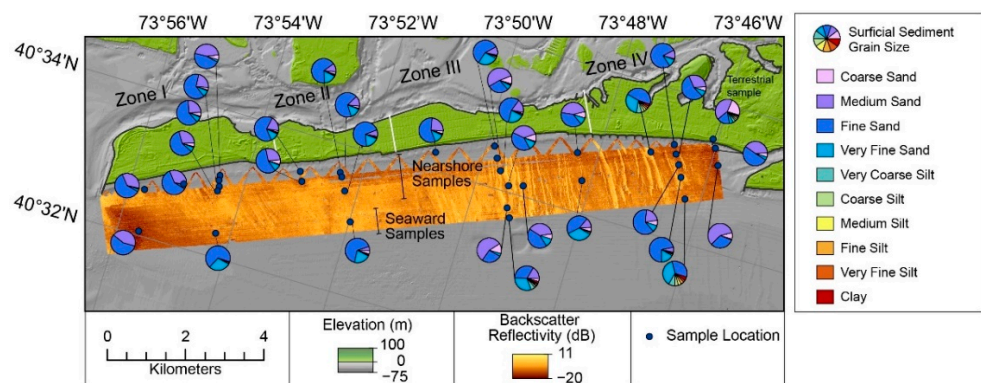


Figure 7. Grain size of surficial sediment samples are shown over the multibeam backscatter map. Locations of samples are shown by dark blue circles. Colors within the pie charts indicate the proportions of sand, silt, and clay.

Finally, to support our interpretations of Holocene stratigraphy, we downloaded and georeferenced NOAA Historical Map and Chart Collection (historicalcharts.noaa.gov, accessed on 7 February 2021) maps from the Rockaway Peninsula. We georeferenced these maps using ground control points and digitized shorelines in ArcMap 10 (Figure 2A,B).

4. Results

4.1. Seafloor Morphology and Texture

Multibeam bathymetry and backscatter reveal several features: a smooth nearshore and shelf in the west, increasing patches of roughness in the central peninsula, and elongate bedforms and an ebb-tidal delta in the east (Figures 4A and 5). Based on surficial bedforms (described in this section), multibeam backscatter (described in this section), sediment

thickness (discussed in Section 4.2.3), and subbottom channel geometry (described in Section 4.2.2), the peninsula was divided into four geomorphic zones, with zone I in the west and zone IV to the east (Figures 4A and 5). A large shoal adjacent to the west Rockaway jetty is the most prominent feature in zone I. Maps of bathymetry and bathymetric slope (Figure 4A,B) reveal that the shoal is covered with ripples, has the lowest backscatter reflectivity in the survey (Figure 5), and is dominated by fine sand (Figure 7). Zone II is smooth and featureless in comparison to the other zones. Abrupt increases in depth at the seaward extent of multibeam coverage in zone III indicate borrow sites for beach nourishment (Figure 4A). Roughness and slope increase in zone III, where linear, shore-perpendicular bedforms are present, displaying 1–2 m of relief, and resulting in patchy and discontinuous sediment cover (Figure 4B). The map of bathymetric slope reveals that bedforms are asymmetric with steeper flanks to the east. Bedforms are most noticeable in backscatter maps, where low-amplitude bedform peaks are separated by high-amplitude troughs (Figure 5). Zone IV is dominated by the ebb-tide delta at the mouth of the East Rockaway Inlet, which creates a prominent shoal, the west side of which is blanketed by linear surficial bedforms with high backscatter reflectivity (Figures 4 and 5).

We interpret the linear, high-backscatter features as sorted bedforms (SB) [55–57]. Like features described offshore of Watch Hill on Fire Island [5,8], the features we mapped also exhibit higher backscatter on the eastward-facing ridge flanks relative to the troughs (Figure 5). Surficial grain size samples reveal bedform troughs with high backscatter have the coarsest surficial sediment, whereas sediment from bedform peaks with low backscatter have less coarse and medium grained sand (Figure 7). SB morphologies in our study area vary with sediment thickness, such that SB in zone IV are fewer in number and have longer wavelengths, whereas SB in zone III are more abundant and have mixed short- and long wavelengths (Figure 5).

Shoreface morphologic variability along the margin is also observed in cross-shore bathymetric profiles (Figure 6). Shoreface and shelf profiles in zone I exhibit the greatest range in profile morphologies, which is attributed to the presence of a nearshore bar at cross-shore distances of 100–300 m in the eastern portion of zone I and accumulation of sediment updrift of the western Rockaway jetty at cross-shore distances between 600–2000 m (Figure 6A). Zones II and III have lower standard deviations in shoreface elevation, which suggests more uniform alongshore morphology within these zones. Zone IV has low bathymetric standard deviations and less morphologic variability at shallow depths (0–200 m distance), but morphologic variability increases seaward due to eastward-thickening ebb-tidal delta deposits. Filtered alongshore averaged shoreface gradients reveal variability in shoreface steepness along the margin, with upper shoreface slopes decreasing from east to west. Additionally, maximum shoreface slopes occur at variable distances from the shoreline; maximum slopes are the most landward in zone IV and the most seaward in zone I (Figure 6E).

Surficial sediment grain size samples are dominated by medium and fine sand, with minor traces of coarse and very fine sand (Figure 7). Seaward fining trends are also observed, with nearshore samples containing 16% more medium sand on average than seaward samples, and seaward samples containing 17% more very fine sand on average than nearshore samples. Zones I and III have the coarsest sediment, with average D_{50} around 210 μm , although zone III has higher percentages of coarse and medium sand [54]. An eastern source of coarse sediment may be terrestrial sediment, since a terrestrial sample collected from beneath the undercut boardwalk in zone IV is coarser than all of the marine samples, with 23% coarse sand and a D_{50} of 338 μm [54]; however, more terrestrial samples are required to confirm this. Within zone III, the coarsest samples are located in sorted bedform troughs with high backscatter, with average D_{50} of 278 μm and 11% coarse sand. Zone II has the finest sediment, with average D_{50} of 175 μm and samples have an average of 63% fine sand.

4.2. Seismic Stratigraphic Framework
 4.2.1. Regional Unconformity

The most prominent feature in the chirp seismic profiles is the regional unconformity (RU; indicated by the green line in Figures 8–11). It separates an upper unit containing reflections with spatially-variable amplitude (see Section 4.2.3) from a lower unit that consists of acoustically transparent sediment incised by channels that are infilled with sediment with low-medium amplitude dipping reflections (Figure 8). The lower boundary of the acoustically transparent, basal unit could not be detected in chirp profiles due to lack of penetration (Figure 8). RU can be traced along the entirety of the survey area and dips westward and seaward (Figures 8 and 9). RU is observed well below the seafloor in zones I and II (Lines 12 and 25; Figure 8A,B and Figure 9) whereas in eastern zones III and IV, it shoals, sometimes merging with the seafloor. In portions of zone III and western zone IV, RU appears to undulate subtly where it is blanketed by sorted bedforms (Figures 10 and 11). This suggests that sorted bedform migration may be actively modifying the morphology of RU where it intersects the seafloor.

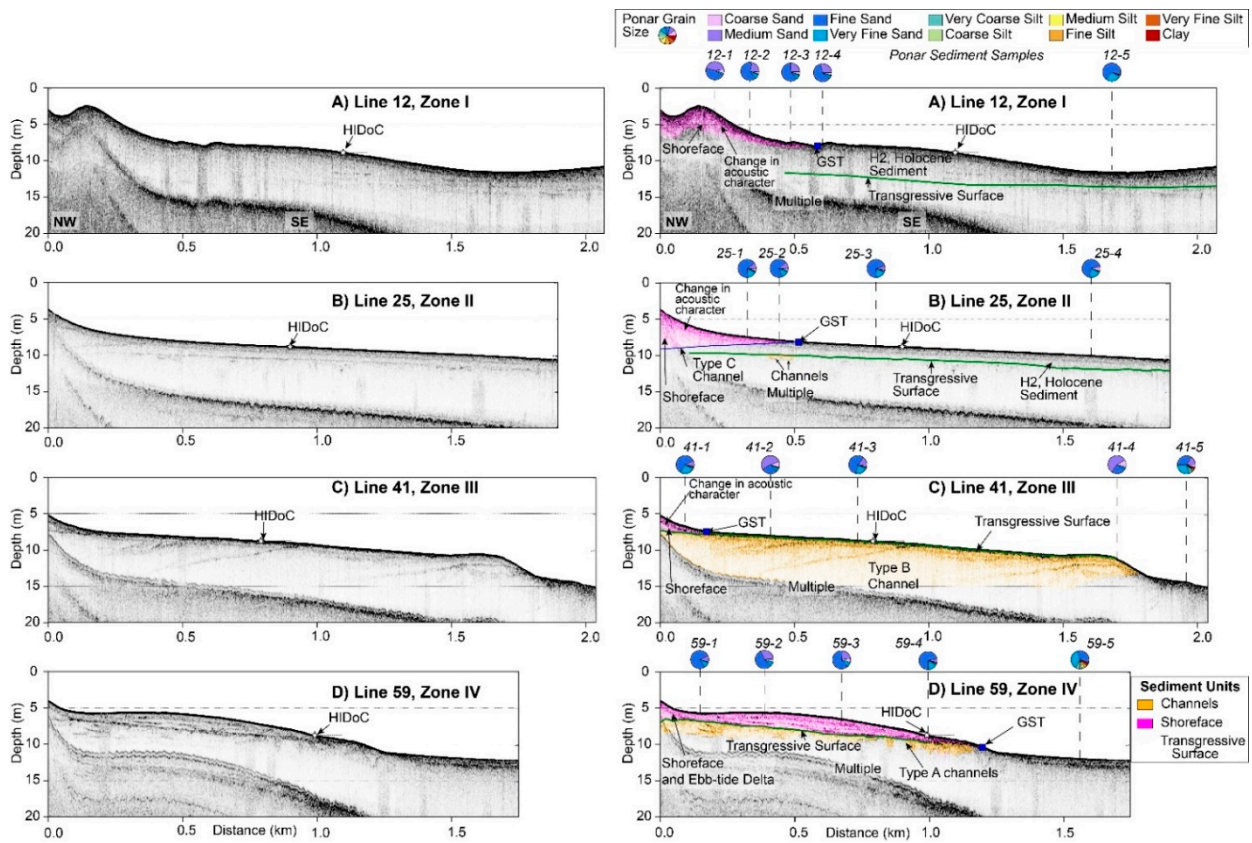


Figure 8. Uninterpreted (left) and interpreted (right) dip profiles from each of the four geomorphic zones highlight variable shoreface morphology across the peninsula. (A) Line 12, (B) Line 25, (C) Line 41, and (D) Line 59. Dashed black lines show the location of surficial sediment grabs; grain size composition is shown by colored wedges; and italic numbers above grain size composition are sample names referenced in Sections 4.2.2 and 4.2.3. GST = Geologic Shoreface Toe. HIDoC = Hallermeier (1981) inner depth of closure. Profile locations are shown in Figure 1.

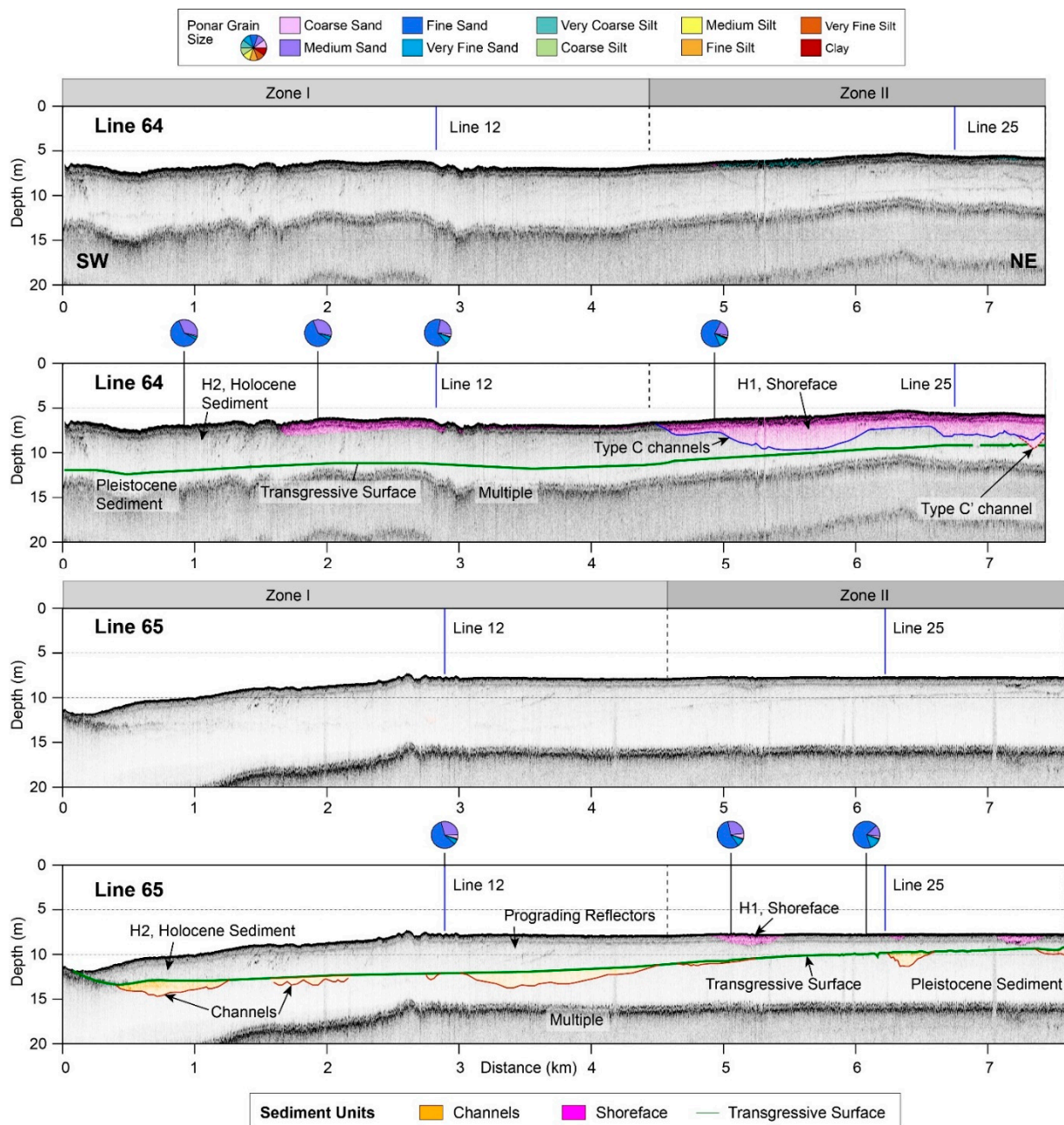


Figure 9. Nearshore strike profile 64 and seaward line 65 within the western geomorphic zones I and II highlight along-margin variability in depth of the regional unconformity and shoreface unit thickness. Solid black vertical lines show the location of surficial sediment grabs and grain size composition is shown by colored wedges. Blue vertical lines indicate intersecting dip profiles shown in Figure 8A,B. Profile locations are shown in Figure 1.

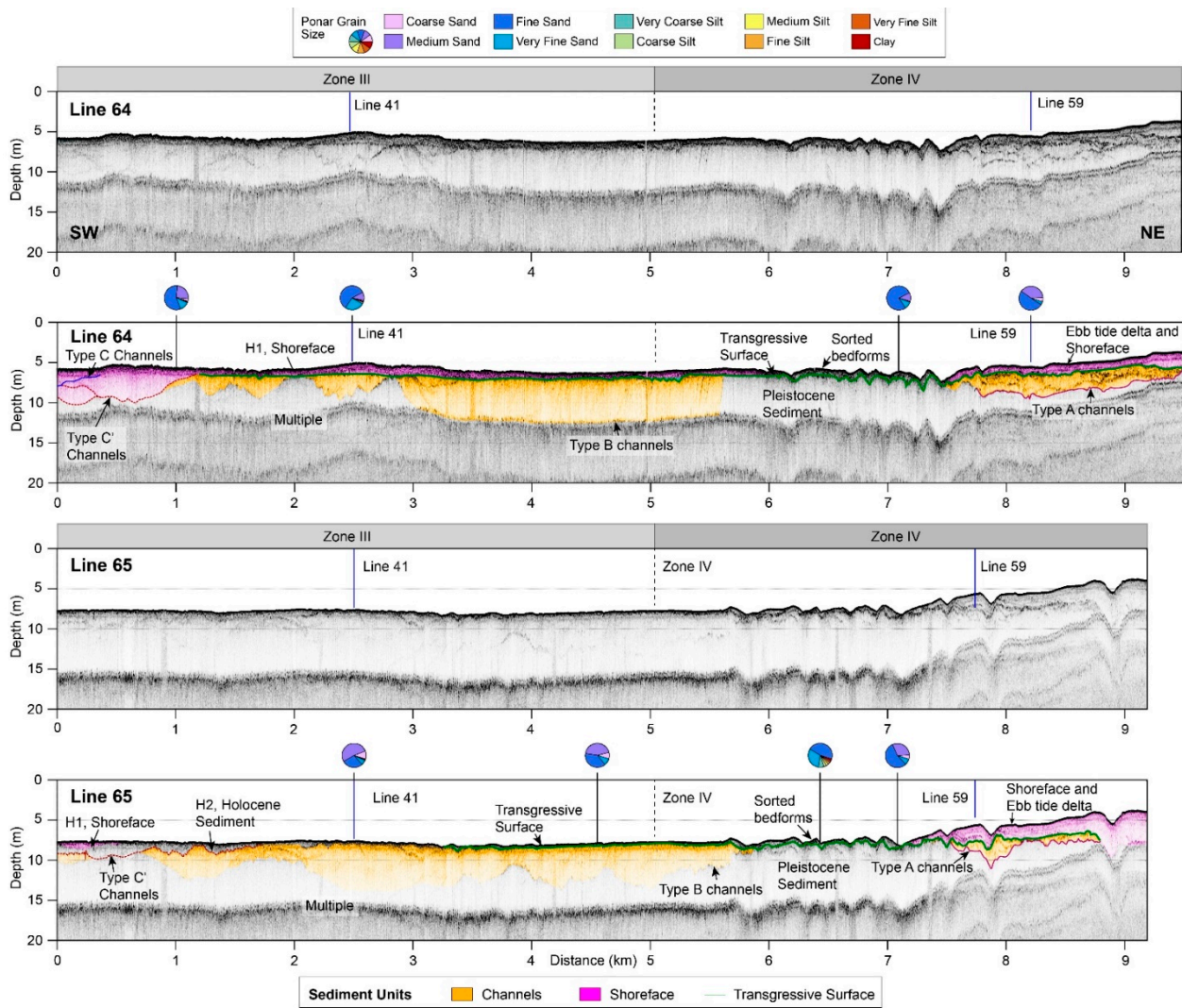


Figure 10. Nearshore strike profile 64 and seaward line 65 within the eastern geomorphic zones III and IV highlight along-margin variability in shoreface units, type B channels, and ebb tide delta deposits. Solid black lines show the location of surficial sediment grabs and grain size composition is shown by colored wedges. Blue vertical lines indicate intersecting dip profiles shown in Figure 8C,D. Profile locations are shown in Figure 1.

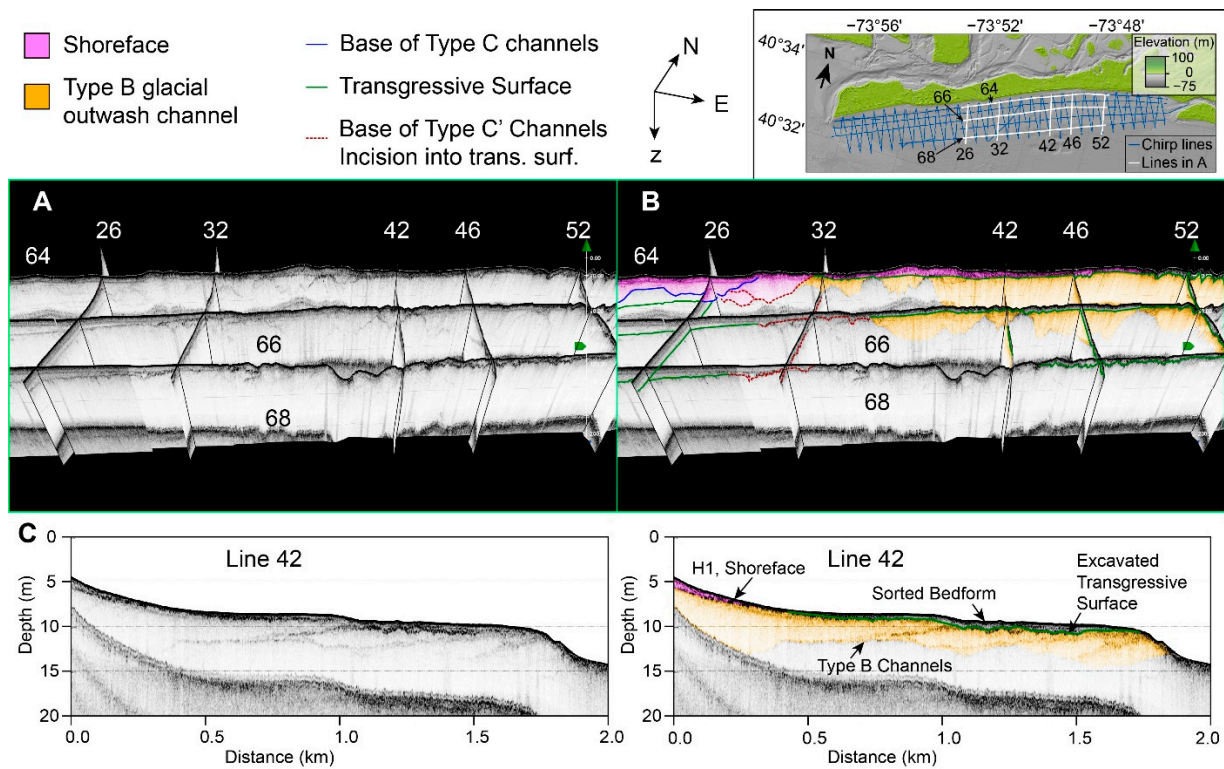


Figure 11. (A,B) Uninterpreted and interpreted seismic fence diagrams show relationships between the shoreface, the transgressive surface, and underlying Type B, C, and C' channels. Colors are explained in upper left. Location of lines shown in the fence diagrams are shown in the upper right. (C) Uninterpreted and interpreted profiles of dip profile 42 highlight extensive Type B channels and areas where the transgressive surface is excavated by a sorted bedform.

4.2.2. Sub-Seafloor Channels

Three main channel morphologies are observed in the subsurface (Figures 9 and 10). Type A channels are located at the mouth of the East Rockaway inlet in zone IV (Figures 8D and 10). Type A channels have the lowest channel height, where channel height is defined as the vertical distance from the channel thalweg to the overlying RU. Thin type A channels exhibit cross-cutting relationships and are infilled by acoustically transparent sediment (Figures 8D and 10). The tops of these channels are truncated by an irregular, undulatory unconformity that is overlain by sediment deposits that thicken towards the inlet (Figure 10).

Type B channels are present in geomorphic zones III and IV and are broad, deep features infilled with acoustically transparent sediment interspersed with low-medium amplitude reflections (Figures 8C and 10). Where observed, the basal boundary of type B channels is undulatory (Figure 10). In dip profile 41, internal reflections within type B channels dip landward (northward; Figure 8C). In strike lines 64 and 65, there are faint, west-ward-dipping reflections suggestive of landward (northward) and westward channel migration (Figure 10). It is possible that samples 41-2 and 41-4 collected along dip line 41 may have sampled type B channel sediment, since they are dominated by medium and fine sand with some coarse fractions, making them coarser than other samples along line 41 (41-3 and 41-5; Figure 8C). It is possible that these finer samples (41-3 and 41-5) recovered material from a thin veneer sediment overlying Type B channels (Figure 8C).

Subsurface channel geometry becomes increasingly complex west of type B channels. Type C' channels represent a transition between type B and C channels (Figures 9–11). These channels cross-cut older type B channels in strike line 64 and the basal boundary incises into and obscures the RU (Figures 10 and 11). This relationship suggests that type C' channels are younger than type B channels. Seaward on strike lines 66 and 68,

type C' channels incise into and increase the rugosity of the RU, with the greatest incision in landward line 64 and diminishing type C' channel heights in seaward lines 66 and 68 (Figure 11).

Type C channels truncate type C' channels and incise into the unit above RU and RU itself (Figures 9 and 11). We distinguish type C channels from type C' channels by their spatial extent and the truncation of type C' channels by type C channels. Unlike type C' channels, type C channels are not observed to extend across the shoreface and do not incise into the RU seaward of strike lines 65, 66, and 68 (Figure 11). These channels exhibit multiple instances of overprinting in a westerly direction, have low relief (~1–6 m), and are infilled by acoustically transparent sediment (Figures 9 and 11). These characteristics and incision into type C' channels suggest that type C channels represent western channel migration and are younger than C' channels. In dip profile 25, the basal boundary of type C channels defines the base of the shoreface reflection on top of which shoreface sediment downlaps (Figure 8B).

4.2.3. Upper Unit and Shoreface Stratigraphy

The upper unit is bounded at its base by RU and at its top by the seafloor. Therefore, features with positive bathymetric expression increase the volume of the upper unit, such as the nearshore bars in zones I and II, the ebb-tide delta in zone IV, and sorted bedforms in zones III and IV. It exhibits along-margin variability in acoustic character. In eastern zone IV, sediment within the ebb-tide delta contains conformable internal reflections with moderate amplitudes (Figure 9). In central zone II, the upper unit is acoustically transparent, whereas in western zone I, the upper unit contains westward-dipping reflections with low to moderate amplitude (Figure 8A). The eastward shoaling of the RU results in thinning upper unit deposits, the thinnest of which were found in zone III (Figures 8C and 10). Despite being similarly limited from the subsurface, upper unit sediment thickness in zones III and IV is remarkably different due to the ebb tidal delta in zone IV (Figures 8 and 10).

In some chirp profiles, the landward portion of the upper unit is dissected by a reflection surface, effectively dividing it into two parts, where H1 is bounded by the seafloor and that reflection surface and H2 is bounded by that reflection surface and RU. Though not always observed, this reflection surface exhibits a range of acoustic amplitudes, with weak amplitudes in line 12, moderate amplitudes in line 25, and higher amplitudes in lines 41 and 59 (Figure 8C,D). Given the landward location of this reflection surface and its position within the section, we interpret this as a basal shoreface reflector, separating reworked H1 sediments above from un- or less-disturbed H2 sediments below. Where distinct from RU, the depth and morphology of the basal shoreface reflector is the primary control on H1 thickness. On line 25 in zone II, the base of the shoreface appears to be controlled by underlying type C channels (described in Section 4.2.2) and dips towards the north resulting in H1 units that thicken toward the shoreline (Figure 8B). Westward, in zone I, the basal shoreface reflection, where present, is vertically separated from the RU by westward prograding sediments in underlying H2 (Figure 8A) and is independent from any subsurface channel features, suggesting that this basal reflection was generated from sediment sorting within the seabed. In zones III and IV, the basal shoreface reflection coincides with RU, resulting in thin H1 units (Figure 8C,D).

The acoustic characteristics of unit H1 vary along the margin. In line 12, low amplitude seaward-prograding internal reflections are observed throughout H1 (Figure 8A). In zones II, III, and IV, low amplitude, closely spaced, discontinuous, and chaotic reflections are observed in the upper portion of H1. In general, the lower part of H1 in zones II and IV is acoustically transparent (Figure 8B,D), whereas in zone III it has a few faint, chaotic internal reflections (Figure 8C). These differences in acoustic character between the upper and lower parts of H1 can be observed in seismic profiles in Figure 8, but because they are not spatially consistent alongshore, we choose not to divide H1 into two separate units. The contribution of units H1 and H2 to upper unit sediment thickness varies along the margin in accordance with accommodation from the overall dip of the RU surface, as well

as channels and features with positive morphology [58]. In some zones (III and IV), H1 comprises the entirety of upper unit sediment, and in other areas (zones I and II), only a portion (Figure 8) [58]. Upper unit sediment is thinnest within zone III, where it is mostly composed of H1; at seafloor depths greater than ~7 m, upper unit sediment is sparse and varies from 0 to 2 m with the presence/absence of sorted bedforms (Figure 8C). In zone IV, the upper unit deposit displays moderate thickness even though RU is much higher in the section there, because it is dominated by the presence of the ebb-tide delta (Figure 12A). Where the RU is deeper in zone I, H2 sediments dominate upper unit sediment thickness due to increasing accommodation and the accumulation of sediment updrift of the western Rockaway jetty that was constructed in the 1930s (Figures 8A, 9 and 12A). As a result of these geologic and morphologic controls, H2 volume exhibits more variability than H1 volume [56]. In summary, variability in the thickness of the upper unit (H1 and H2) can be related to the westward-dipping RU, features with positive morphology, and anthropogenic modifications.

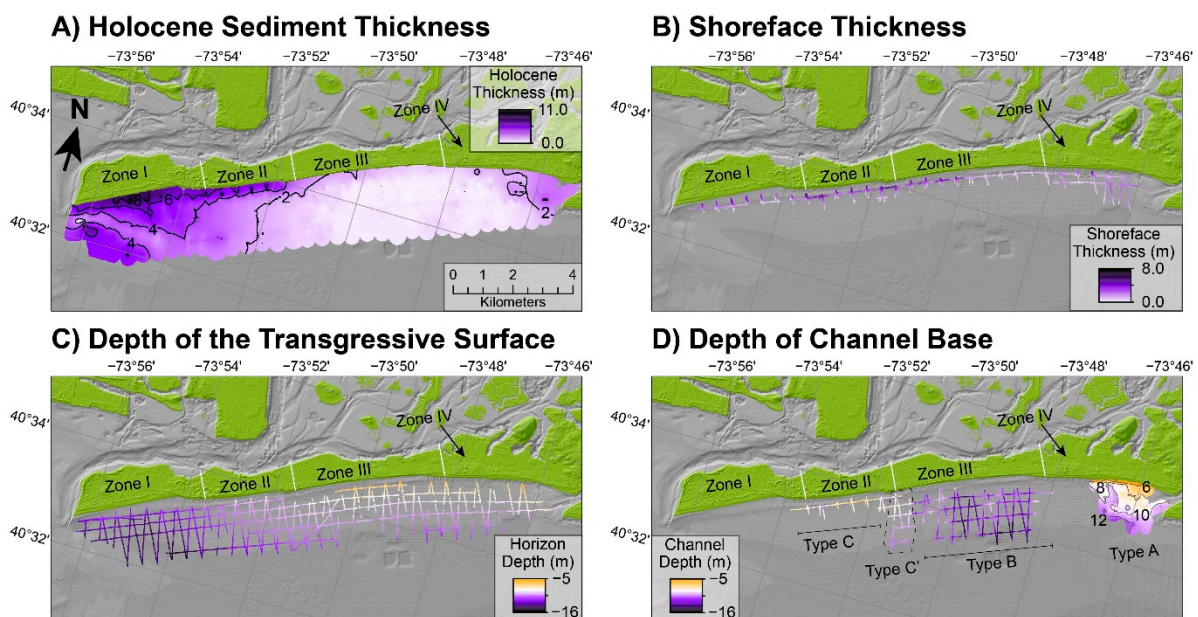


Figure 12. Isopach and Structure maps. (A) Interpolated thickness map of Holocene sediment. (B) Thickness of Shoreface sediment. (C) Structure map of the depth of the transgressive surface. (D) Structure map of the depth of Type C, C', B, and A channels. White lines on the peninsula delineate the boundaries of the geomorphic zones.

Upper unit sediment in H1 is dominated by fine to medium sand and is moderately well sorted (Figures 7 and 8). Only one sample from the shallow portions (<5 m depth) of H1 was recovered along dip line 12 (sample 12-1) and this sample is coarser than two samples from deeper portions of H1 (Samples 12-2 and 12-3; Figure 8A). This finding corroborates previous studies that observed changes in grain size between the shallow and deeper portions of the shoreface [59]. More samples were recovered from deeper portions (>5 m depth) of H1. Among them, deeper H1 samples in zone I have the coarsest D_{50} of 207 μm (Samples 12-3 and 12-4), whereas deeper H1 samples in zone II have average D_{50} of 170 μm (25-1 and 25-2), and in zone III, deeper H1 samples have D_{50} of 151 μm (41-1; Figure 8). The ebb tide delta in zone IV exhibits the largest variability in grain size, with D_{50} ranging from 160 to 211 μm (Samples 59-1 to 59-4; Figure 8D). On average, H1 sediment is coarser than H2 sediment, as H2 samples 12-5, 25-3, and 25-4 from the westward prograding package contain higher proportions of fine sand and lower proportions of medium sand (Figure 8A,B).

4.3. The Geologic Shoreface Toe and Comparisons to Other Estimates of Shoreface Extent

We interpret the intersection of the basal shoreface reflection with the seafloor as the geologic shoreface toe (GST), which represents the seaward boundary of the shoreface unit (H1; Figure 8). GST depths in zone IV spanned the largest range (~6.5–9.5 m) and were deepest on average, since their depth and extent are controlled by the ebb tide delta deposit (Figure 13). Outside of zone IV, the average GST depth was ~7.2 m (Table 1). GST depths throughout zone II had the second-highest variability since Type C and C' channels control the depth of the basal shoreface reflection and their cross-shore extent varies alongshore (Figure 13). In zone III, GST depth varies even when shoreface width is uniform because of undulatory sorted bedforms. GSTs were not widely mapped in zone I due to difficulty mapping a basal shoreface reflection separate from the regional unconformity, and the lack of GST identified likely contributes to low r^2 values for zone I in Table 1. Shoreface widths were calculated as the distance from the mean high water (MHW) shoreline (0.46 m) to the GST. Average shoreface width was largest in zone IV where the shoreface spanned the ebb tidal deposit (Figure 13). Elsewhere along the peninsula, shoreface widths averaged ~420 m, though the narrowest average shoreface widths were observed in zone III with an average of ~390 m. Relatively shallow GSTs and narrow shoreface widths combined to steepen the shoreface in zones I, III, and the western portion of IV.

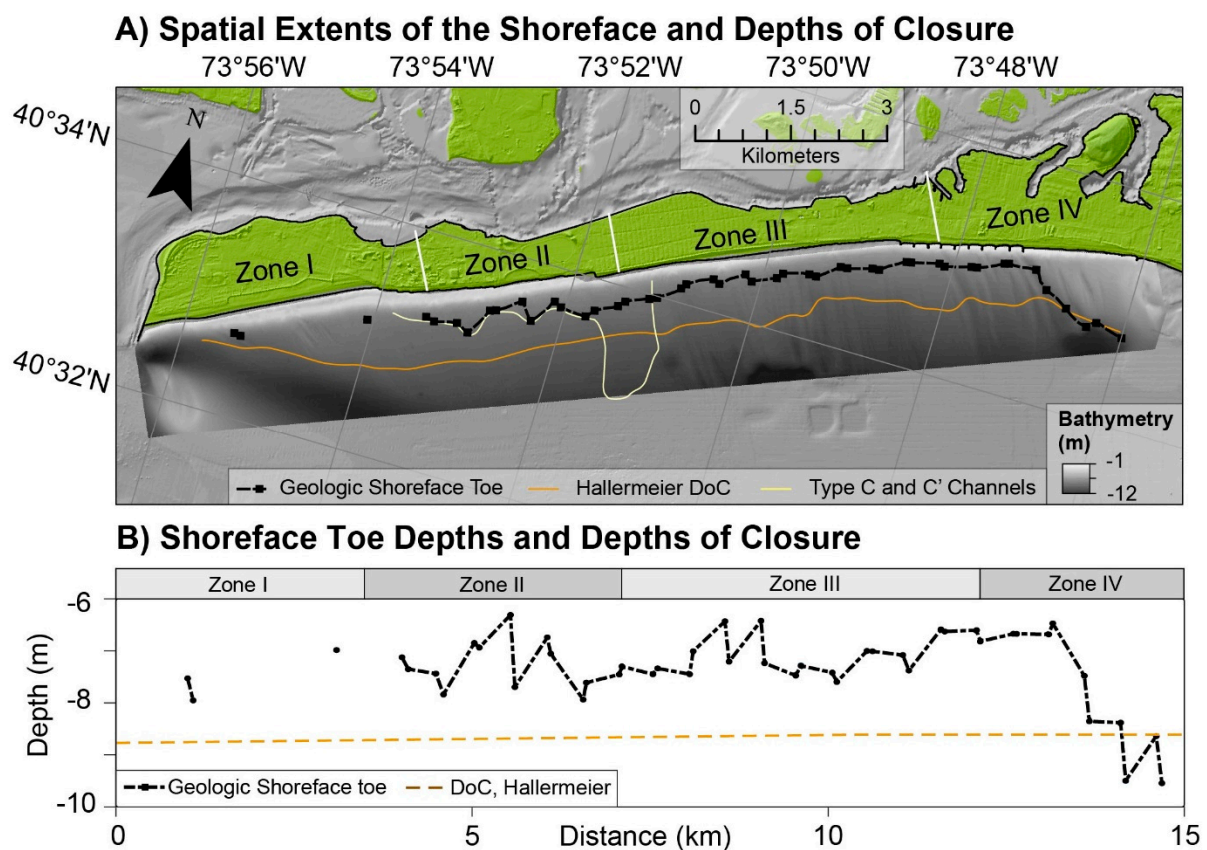


Figure 13. (A) Spatial extents of the geologic shoreface toe and Hallermeier [60] inner depth of closure (DoC) are superimposed on a map of bathymetry. The extent of type C and C' channels are spatially coincident with widening shorefaces in zone II. (B) The depths of geologic shoreface toes are plotted with the Hallermeier [60] inner depth of closure.

Table 1. Average geologic shoreface toe (GST) depth and average shoreface volume in each zone. Shoreface volume estimates are modified from Wei et al. [58]. Relationships between GST depth compared to shoreface width and shoreface volume.

Zone	Average GST Depth (m)	Average Shoreface Volume ($1 \times 10^3 \text{ m}^3/\text{m}$)	R ² , GST Depth vs. Shoreface Width	R ² , GST Depth vs. Shoreface Volume
I	7.39	0.62	0.29	0.0098
II	7.24	1.02	0.89	0.92
III	7.14	0.38	0.76	0.028
IV	7.65	1.13	0.92	0.83
Entire peninsula	7.45	0.73	0.83	0.63

When compared for the entirety of the peninsula, deeper GSTs corresponded to wider shorefaces ($r^2 = 0.83$), but the relationships varied by zone (Table 1). There was a weak relationship between GST depths and shoreface width in zone I ($r^2 = 0.29$). The strongest relationships between GST depth and shoreface width were found in zones II ($r^2 = 0.89$) and IV ($r^2 = 0.92$), but still involved some scatter, and, in the case of zone IV, was likely related to the eastward widening ebb tidal delta deposit. We then compared GST depth to shoreface volumes published by Wei et al. [58], which were calculated by integrating sediment thickness between the base of the shoreface reflection and the seafloor. A weak relationship between GST depth and shoreface volume was found in zones I and III ($r^2 = 0.0098$ and 0.028 , respectively), whereas comparisons in zones II and IV yielded a stronger correspondence between deeper GST depths and larger shoreface volumes ($r^2 = 0.92$ and 0.83 , respectively).

Since we interpret the GST as the geology-based boundary for shoreface extent, we compare it to other derivations of shoreface extent, principally the depth of closure (DoC). We used two formulations to calculate the DoC at Rockaway, using hydrodynamic information from U.S. Army Corps of Engineers Wave Information Studies station 63125 [47], including the inner and outer DoC based on Hallermeier [60], which are 8.77 and 23.31 m respectively. Inner DoCs derived from Hallermeier’s formulations use average wave parameters to estimate hydrodynamic processes on engineering timescales (10^0 – 10^1 years) [60] and are hypothesized to represent the offshore limit of reworking of the shoreface by waves, assuming no influence from geology or anthropogenic impacts. Since the Hallermeier formulation does not include a grain size term, it could serve as a useful tool for teasing out the influences of wave height and period on DoC. Estimated DoCs are compared to spatial-averaged GST depths in Figure 13 and are also plotted on our chirp profiles in Figure 8, with the exception of the Hallermeier outer DoC, the depth of which exceeded survey extent. On average, GSTs for each zone are shallower than the inner Hallermeier DoC estimate (Figure 13), suggesting that the shoreface at Rockaway responds on very short time scales. In eastern zone III and western zone IV where the coast is modified by a groin field, the GST shoals (Figure 13), suggesting that anthropogenic modifications may shorten the timescales of shoreface response.

5. Discussion

In this study, we explored how the combined influences of shoreface geology, barrier island evolution, and human intervention contributed to spatial variations in shoreface sediment availability along the Rockaway Peninsula. We found that along-margin variability in accommodation and natural and human-mediated morphologic features were the primary controls on shoreface sediment availability. Additionally, we explored the time scales over which fluxes from the shoreface will contribute to barrier island behavior by comparing shoreface extent derived from our data to estimates derived from empirical wave-based formulations. Below we discuss our stratigraphic interpretations (5.1), controls

on variability in shoreface sediment availability (5.2) and extent (5.3), and the implications of our findings for along-shore varying response to future storms and sea level rise.

5.1. Stratigraphic Interpretations

Sediment units observed in chirp seismic profiles are interpreted based on their relative position to the westward-dipping RU. We interpret the RU as the transgressive surface, which separates Pleistocene sediments below it from Holocene sediments above it (Holocene sediment includes H1 + H2). Sediment below the RU was likely deposited during a relative sea-level highstand preceding Marine Isotope Stage (MIS) 2. During the sea-level lowstand of MIS 2, type B channels incised and eroded sediment below the RU, and as sea-level rose following the lowstand, channels were infilled. The RU was formed during the sea-level transgression, during which wave-based erosion truncated the tops of type B channel infill. Similar sediment geometries have been observed in the nearshore and shelf elsewhere in the New York bight [e.g., 5,8,53] and elsewhere along the east coast [1,61–64]. Hereafter, we will present our interpretations and discuss the processes that formed them starting from the oldest units (Pleistocene channels) to youngest (late Holocene).

The morphology of the three channel types and their stratigraphic position relative to RU suggest that they are diachronous and likely formed by different processes. The oldest channels are likely type B channels, since their position below the RU suggests they were formed before the last sea-level transgression. Type B channels are spatially coincident with a gap in the Harbor Hill Moraine, which suggests that type B channels are an extension of glacial outwash Channel D identified by Williams [34]. Similar glacial outwash channels are also observed offshore of Fire Island [61]. The deepening of the transgressive surface in the west coupled with the absence of channels with similar morphologies below RU there suggests that type B channel infill is less erodible than sediment below RU in the west. This is corroborated by sediment samples 41-2 and 41-4 that recovered coarser sediments where type B channel infill is exposed at the seafloor. In zones I and II where type B channels are absent, more erodible Pleistocene sediment allowed for a deepening of the transgressive surface resulting in increased accommodation, which is a primary control on shoreface sediment availability and morphology.

Type C and C' channels are likely much younger than type B channels since they incise into Holocene sediment and the transgressive surface. Historic maps from the 18th and early 19th centuries reveal the end of the peninsula was in a more eastward position [42,65], and between 1835 and 1889, the end of the Rockaway peninsula advanced within the boundaries of type C and C' channels (Figure 2A), suggesting that these channels could have been incised by tidally-driven flows around the western end of the peninsula and subsequently infilled. Channels similar to type C and C' channels were observed below the shoreface at Fire Island, NY by Liu and Goff [66], who interpreted cross-cutting channel reflections as migrating inlet channels. Historical shoreline analysis and the variable depth of type C/C' channels suggests a slightly different process here. Temporally-variable peninsula growth rates (Figure 3) help explain differences in depth and extent of C and C' channels. The period of slow growth from 1835–1866 allowed type C' channels to incise into the underlying substrate for a longer period, deepening the incisions and allowing them to extend further offshore (Figures 10 and 11). Similarly, rapid periods of peninsula progradation between 1866–1879 may have shortened the time periods of type C channel incision, resulting in channels confined to the shoreface with limited seaward extent (Figure 11). West of the 1889 shoreline, deepening of the transgressive surface may have triggered a shift from inlet incision and infilling to progradation of the barrier spit and the associated shoreface, which could explain the lack of Holocene channels to the west of type C channels. Thus, the geometry of type C and C' Holocene shoreface channels depended on accommodation, underlying substrate, and the duration of incision.

Type A channels are likely the youngest channels and we interpret that type A channels and the overlying ebb-tidal delta in east Rockaway represent natural and human-mediated

inlet incision and deposition, respectively, since the 19th century. First, the East Rockaway Inlet migrated west as Long Beach Island rapidly prograded during 1835–1860 [67], and inlet migration initially formed small type A channels. After 1865, these channels were filled in to create Hog Island, a recreational beach that was destroyed during a hurricane in 1893 [67]. We hypothesize that the hurricane may have excavated younger type A channels and reworked sediment from Hog Island. After hurricane passage, this reworked material may have been deposited with conformable reflectors into type A channels. Such rapid emplacement of material could explain the irregular boundary of type A channels that appear to represent scouring events (Figure 10).

Changes in transgressive surface elevation and the alongshore position and depth of sub-seafloor tidal channels define the base of the shoreface unit. The base of the shoreface is most easily identified in zones III and IV, where it coincides with the transgressive surface at or near the seafloor and appears to be modified by sorted bedform migration. In zones I and II, where the transgressive surface is lower in the section, we identified other reflections within the Holocene package (e.g., above the transgressive surface) that we interpret as the basal shoreface reflection. In zone I, where sediment availability is higher, wave ravinement is likely the primary mechanism for the formation of basal shoreface reflections where they are observed [68]. In contrast, the basal shoreface reflection in zone II is defined by relict tidal channels, the depth and extent of which increase the volume of sediment toward the island (see discussion of Type C/C' channels above). These observations demonstrate that the base of the shoreface represents a variety of processes and may not necessarily mark the transition from offshore marine sedimentation below to shoreface sedimentation above [59]. Furthermore, our results suggest that the transgressive surface alone may not reflect the true volume of shoreface sediment, as has been interpreted elsewhere [5,69,70].

Wave ravinement may also affect the internal stratigraphy of the shoreface unit, which is observed in profiles from western Rockaway where sediment availability is higher. For example, in some profiles from zone II, we were able to resolve somewhat chaotic acoustic characteristics within upper portions of the shoreface unit that separated what we interpret as reworked portions of the unit from lower undisturbed parts of tidal channel infill (Figure 8B). These acoustic distinctions within the zone II shoreface unit (H1) coupled with the undisturbed Holocene sediment below it (H2) may be similar to the upper shoreface, proximal lower shoreface and distal lower shoreface units described in East Texas [59,71], though we don't have cores to confirm whether there are sedimentological differences between units as observed in Texas. However, the slightly coarser grain size of sample 12-1 relative to 12-2 and 12-3 may be evidence that shallow, wave-based reworking is occurring in the zone II shoreface as well. (Figure 8A). We hypothesize that wave ravinement may serve as a mechanism for these changes in acoustic character and grain size. Furthermore, the data suggest that the current wave climate may be reworking only a small fraction of the available sediment in western Rockaway and that future wave ravinement of the shoreface has the potential to liberate much more sediment in western Rockaway than in eastern Rockaway.

5.2. Shoreface Sediment Availability and Implications for Cross-Shore Sediment Fluxes

Recent work has highlighted the need for more detailed information about shoreface morphology and geology to improve forecasts of shoreline position with rising sea level [10,11], to improve understanding of mesoscale barrier island response to changes in climate and sediment supply [72], and to better understand sediment transport between the upper and lower shoreface and the beach [73]. Our results address this need and do so at a spatial resolution that improves upon earlier assessments of shoreface geology [24,59,69–71]. The data reveal complexity in the stratigraphy of the shoreface units and their relationship to the Holocene-Pleistocene boundary, which provide insight into the competing controls on shoreface sediment availability and where there may be significant volumes of sediment for the coastal system in the future. Further, the data demonstrate that

the Holocene-Pleistocene boundary alone may not be the best baseline from which to assess shoreface sediment availability, particularly over shorter timescales (10s–100s of years).

The simplest relationship between the Holocene-Pleistocene boundary and shoreface sediment availability is observed in zone III, where shoreface sediment availability is driven almost entirely by limited accommodation associated with the morphology of the transgressive surface (described in Section 5.1) as has been reported in several other locations [53,59,70,74,75]. Our data indicate that lateral migration of sorted bedforms may rework underlying type B channel deposits, but we hypothesize that any sediment liberated from this process is unlikely to supply sediment to the shoreface at rates fast enough to keep up with shoreline migration. This is consistent with findings from repeat bathymetry studies at Fire Island which suggest that sorted bedform migration does not contribute significantly to shoreface sediment availability [76]. In total, the data imply that cross-shore fluxes of sediment from the shoreface to the beach have been and will continue to be limited in zone III.

Despite having similarly limited accommodation, shoreface sediment availability in zone IV increases relative to zone III due to local morphology, in this case the ebb tidal delta associated with the East Rockaway inlet, which is similar to features adjacent to Bolivar Roads Inlet on the East Texas shelf [59,71,77]. Due to the cross- and alongshore extent of this feature, zone IV shoreface sediment availability is the highest we observed. Nevertheless, the ebb tidal delta is likely in equilibrium with inlet processes and it is not clear to what extent this deposit supplies the beach onshore of it.

In contrast to zones III and IV, sediment availability is enhanced in zones I and II, and as a result, the cross-shore sediment fluxes may be more influenced by the efficiency of the wave climate rather than geology. In zone II, infilled tidal channels increase Holocene and shoreface sediment availability. Further west, in zone I, where Holocene sediment is relatively unlimited due to the deepening transgressive surface, the primary limitation on cross-shore exchange of sediment between the shoreface and the beach is the efficiency of the wave climate in liberating and transporting reworked deposits. With continued shoreface ravinement, future fluxes from the shoreface in zones I and II will continue to be elevated relative to other regions along the peninsula, particularly during storms when wave conditions can mobilize more sediment from within the shoreface and from beyond the GST. This highlights the limitations of using only the basal shoreface reflection and GST to approximate shoreface sediment availability: the volume of sediment actively contributing to littoral transport may extend beyond the limits of the geologically-defined shoreface unit boundary. Although assessing the combined role of positive morphologic features and sub-seafloor geology in influencing shoreface sediment volumes is not new [3,53,59], this is perhaps the first time significant variability in both has been shown to result in dramatic alongshore differences in shoreface sediment availability over a relatively short span of coastline (<20 km).

Relative to the lower portions of the shoreface (>5 m depth), we suspect that the shallow, upper portions of the shoreface (<5 m depth) reflect feedbacks between shoreface morphology and human modifications more so than geology, at least over timescales of years to decades. First, shoreface morphology and steepness have complicated relationships with sediment availability, varying in both the alongshore and cross-shore domains. The pattern of average upper shorefaces steepening towards the east was surprising given that net longshore transport is to the west and the shoreline is prograding along the western end of the peninsula. Since high sediment supply often results in steeper clinofolds [59,78], we expected that shorefaces in zones I and II would be steeper than eastern shorefaces. One explanation for the disparity between our observations and stratigraphic principles is that upper shoreface morphology in eastern Rockaway reflects human interventions at the shoreline where humans are actively manipulating the barrier system. The steepest shorefaces occur in zones III and IV, where frequent beach nourishment since 1920 (Figure 3) has resulted in long-term shoreline progradation or stabilization, effectively oversteepening the shoreface at its landward boundary. Additionally, groins were constructed between

zones III and IV within the first half of the 20th century to help maintain placed sediments [44,65], further fixing shoreline position and limiting alongshore sediment fluxes. Human-mediated shoreface steepening has also been observed in the Beaufort Sea [79] and on the Irish coast [69] creating positive feedback between steep shoreface slopes and seaward directed sediment transport [73,79–81]. At Rockaway, a potential shift to seaward transport in zones III and IV could limit transport from the shoreface to the beach, which could further exacerbate shoreline erosion, though modeling of these shoreface configurations would help to confirm this hypothesis. Thus, our results suggest that human modifications to the subaerial beach influence the morphology of the upper shoreface and may result in behaviors contrary to natural geomorphologic processes in this important transition zone.

5.3. Geologic Shoreface Toe and Comparison to Depth of Closure

Since the basal shoreface reflection is generated by a variety of processes along the Rockaway peninsula, the cross-shore position of the GST can represent the influences of geology, anthropogenic impacts, and/or hydrodynamics. In zone I, where sediment is not limited, the GST likely represents the offshore limit of sediment reworking by waves. This is similar to the findings of Schwab et al. [5,8], who interpreted shoreface toes at Fire Island as the depth approximating storm wave base. However, an important distinction from that work is that the GST in Rockaway zone I do not always coincide with the transgressive surface as the interpreted shoreface toes in Fire Island do. In contrast to the GST in zone I, the location of the GST in zone II is tied to antecedent geology, representing the offshore extent of tidal channelization that occurred as the island migrated westward. This is similar to other locations where the framework geology of the shoreface was the primary control on shoreface sediment availability and extent [53,59,75,82]. Here, the GST represents the offshore limit of the lower boundary of the shoreface sediment reservoir, helping to define the shoreface sediment volume that may be available for the future. Importantly, and particularly during storms, it likely does not represent offshore extent over which sediment is mobilized by average wave conditions. Therefore, we conclude that despite delineating the extent of the shoreface sediment unit, the offshore location and depth of the GST is not necessarily a good indicator of shoreface sediment availability except where the thickness of the Holocene section is limited and the transgressive surface and the basal shoreface reflection coincide, as in zones III and IV.

To understand the timescales over which portions of the shoreface unit are mobilized, we compared the GST to the Hallermeier [60] inner depth of closure (HIDoC). Except in zone IV where the location of the GST is controlled by the ebb-tidal delta, GSTs along the peninsula fell within the depth of the HIDoC (Figure 13), which suggests that the entire extent of the shoreface unit in zones I–III could be mobilized on annual to decadal timescales. In zones I and II, the extent of sediment mobility is unlikely to be confined to just the shoreface unit. In both zones, the GST and Holocene sediment seaward of the GST are shallower than HIDoC (Figure 8A,B), which suggests that this Holocene sediment is capable of being reworked and may contribute sediment to the shoreface unit (e.g., sediment transport from the lower to upper shoreface) during high energy events. This is similar to results from western Fire Island, NY, where onshore sediment transport was observed seaward of the shoreface toe during extreme storm conditions [5,8], though the relationship we observed between sandy shoreface units and the HIDoC suggests that transport from the lower to upper shoreface may be possible even during average wave conditions at our study site. In contrast, in sediment-limited eastern Rockaway (and excluding the ebb-tidal delta), the GST is up to 2 m shallower than HIDoC, and Pleistocene glacial outwash deposits are exposed at the seafloor seaward of the GST, instead of Holocene sediment. This erosional-resistant unit is less likely to supply significant amounts of sediment to the littoral system, thereby reducing or eliminating sediment fluxes from the lower to the upper shoreface. Such a reduction in fluxes from the lower shoreface to the beach might be active on other geologically-controlled shorefaces, such as those where hardgrounds or

rocky outcrops are exposed [11,82,83]. At Rockaway, deficiencies in cross-shore sediment supply are probably further exacerbated by human alterations to the system, such as groins, which limit updrift sediment inputs and may favor offshore sediment transport due to steeper shoreface slopes. Based on previous work, the combination of reduced sediment flux from the shoreface and human alterations could increase barrier island vulnerability to extreme storms and future increases in sea-level rise [15,22], though new modeling that better represents the geomorphologic complexity of the shoreface we observed may be needed to better understand the timing and extent of potential changes in barrier island geomorphic state.

6. Conclusions

Improving predictions of barrier island response to changes in sea-level rise and sediment supply requires more detailed information on how variations in shoreface morphology and geology influence sediment fluxes from the shoreface to the beach. Our work elucidates the competing controls on shoreface sediment availability and identifies where there may be significant volumes of sediment for the coastal system in the future. Using geophysical data to reveal the internal stratigraphy of the shallow shoreface, we extend the knowledge learned from previous studies by providing insights on the timescales of shoreface reworking. Furthermore, we explore how geology and human modifications contribute to variable shoreface sediment availability over a relatively short span of the coastline. We find that:

1. Observed shoreface stratigraphy varies over small spatial scales (0.5–3 km). Accommodation, historical barrier island evolution, and natural and human morphologic features all affect shoreface sediment availability, with the relative influence of any one factor varying along margin.
2. Variability in the Holocene-Pleistocene (H-P) boundary elevation limits the distribution of sediment across the shoreface, likely influencing sediment fluxes from the lower to upper shoreface and beach.
3. Comparisons between the offshore limit of the shoreface as defined by the GST and the empirically derived depth of closure suggest that the geologically defined shoreface is actively being reworked over very short time scales (years to decades).
4. The influence of human beach modifications extends seaward into the upper shoreface and may promote increased steepness of the upper shoreface and seaward-directed sediment fluxes.

Observed shoreface geomorphic variability along the Rockaway Peninsula is likely to result in spatially variable responses to storms and sea-level rise. Therefore, more accurate predictions of coastal change should account for both geologic and human influence on shoreface sediment availability and sediment flux magnitudes, even within coastal cells that span only several kilometers.

Author Contributions: Conceptualization, E.W. and J.M.; methodology, E.W. and J.M.; formal analysis, E.W.; investigation, E.W.; resources, J.M.; writing—original draft preparation, E.W.; writing—review and editing, J.M.; visualization, E.W.; supervision, J.M.; project administration, J.M.; funding acquisition, J.M. All authors have read and agreed to the published version of the manuscript.

Funding: This research was funded by the National Fish and Wildlife Foundation grant number 2300.16.055110 and the U.S. Geological Survey Coastal and Marine Hazards and Resources Program.

Institutional Review Board Statement: Not applicable.

Informed Consent Statement: Not applicable.

Data Availability Statement: Data used in this study are available as U.S. Geological survey data releases. Multibeam bathymetry: (Stalk et al., 2020, <https://doi.org/10.5066/P9WNJSFN>) [48], Chirp seismic reflection: (Forde et al., 2021, <https://doi.org/10.5066/P9ZO8QKJ>) [49], Sediment grain size: (Everhart et al., 2022, <https://doi.org/10.5066/P9FH8ZJW>) [54].

Acknowledgments: The authors thank Arnell Forde for chirp seismic data processing and Noreen Buster for management of chirp and bathymetry data. Scientific reviews by Dan Ciarletta, Phil Werne, and two anonymous reviewers provided constructive feedback that improved the manuscript. Any use of trade, form, or product names is for descriptive purposes only and does not imply endorsement by the U.S. Government.

Conflicts of Interest: The authors declare no conflict of interest.

References

1. Timmons, E.A.; Rodriguez, A.B.; Mattheus, C.R.; DeWitt, R. Transition of a regressive to a transgressive barrier island due to back-barrier erosion, increased storminess, and low sediment supply: Bogue Banks, North Carolina, USA. *Mar. Geol.* **2010**, *78*, 100–114. [[CrossRef](#)]
2. Psuty, N.P.; Silveira, T.M. Global climate change: An opportunity for coastal dunes?? *J. Coast. Conserv.* **2010**, *14*, 153–160. [[CrossRef](#)]
3. Miselis, J.L.; McNinch, J.E. Calculating shoreline erosion potential using nearshore stratigraphy and sediment volume: Outer Banks, North Carolina. *J. Geophys. Res. Earth Surface* **2006**, *111*, 1–15. [[CrossRef](#)]
4. McNinch, J.E.; Miselis, J.L. Geology metrics for predicting shoreline change using seabed and sub-bottom observations from the surf zone and nearshore. In *Sediments, Morphology and Sedimentary Processes on Continental Shelves: Special Publication*; Li, M.Z., Sherwood, C.R., Hill, P.R., Eds.; Wiley-Blackwell: West Sussex, UK, 2012; Volume 44, pp. 99–120.
5. Schwab, W.C.; Baldwin, W.E.; Denny, J.F.; Hapke, C.J.; Gayes, P.T.; List, J.H.; Warner, J.C. Modification of the Quaternary stratigraphic framework of the inner-continental shelf by Holocene marine transgression: An example offshore of Fire Island, New York. *Mar. Geol.* **2014**, *355*, 346–360. [[CrossRef](#)]
6. Valiente, N.G.; Masselink, G.; Scott, T.; Conley, D.; McCarroll, R.J. Role of waves and tides on depth of closure and potential for headland bypassing. *Mar. Geol.* **2019**, *407*, 60–75. [[CrossRef](#)]
7. Cowell, P.J.; Stive, M.J.; Niedoroda, A.; Swift, D.J.P. The coastal-tract (part 2): Applications of aggregated modeling of lower-order coastal change. *J. Coast. Res.* **2003**, *19*, 828–848.
8. Schwab, W.C.; Baldwin, W.E.; Hapke, C.J.; Lentz, E.E.; Gayes, P.T.; Denny, J.F.; List, J.H.; Warner, J.C. Geologic evidence for onshore sediment transport from the inner continental shelf: Fire Island, New York. *J. Coast. Res.* **2013**, *29*, 526–544. [[CrossRef](#)]
9. Sallenger, A.H., Jr. Storm impact scale for barrier islands. *J. Coast. Res.* **2000**, *16*, 890–895.
10. Cowell, P.J.; Kinsela, M.A. Shoreface controls on barrier evolution and shoreline change. In *Barrier Dynamics and Response to Changing Climate*; Moore, L.J., Murray, A.B., Eds.; Springer: Cham, Germany, 2018; pp. 243–275.
11. Kinsela, M.A.; Hanslow, D.J.; Carvalho, R.C.; Linklater, M.; Ingleton, T.C.; Morris, B.D.; Allen, K.M.; Sutherland, M.D.; Woodroffe, C.D. Mapping the shoreface of coastal sediment compartments to improve shoreline change forecasts in New South Wales, Australia. *Estuaries Coast.* **2020**, *45*, 1143–1169. [[CrossRef](#)]
12. Stockdon, H.F.; Holman, R.A.; Howd, P.A.; Sallenger, A.H., Jr. Empirical parameterization of setup, swash, and runup. *Coast. Eng.* **2006**, *53*, 573–588. [[CrossRef](#)]
13. Brenner, O.T.; Moore, L.J.; Murray, A.B. The complex influences of back-barrier deposition, substrate slope and underlying stratigraphy in barrier island response to sea-level rise: Insights from the Virginia Barrier Islands, Mid-Atlantic Bight, USA. *Geomorphology* **2015**, *246*, 334–350. [[CrossRef](#)]
14. Moore, L.J.; List, J.H.; Williams, S.J.; Stolper, D. Complexities in barrier island response to sea level rise: Insights from numerical model experiments, North Carolina Outer Banks. *J. Geophys. Res. Earth Surf.* **2010**, *115*, F03004. [[CrossRef](#)]
15. Lorenzo-Trueba, J.; Ashton, A.D. Rollover, drowning, and discontinuous retreat: Distinct modes of barrier response to sea-level rise arising from a simple morphodynamic model. *J. Geophys. Res. Earth Surf.* **2014**, *119*, 779–801. [[CrossRef](#)]
16. Ciarletta, D.J.; Miselis, J.L.; Shawler, J.L.; Hein, C.J. Quantifying thresholds of barrier geomorphic change in a cross-shore sediment-partitioning model. *Earth Surf. Dynam.* **2021**, *9*, 183–203. [[CrossRef](#)]
17. Riggs, S.R.; Cleary, W.J.; Snyder, S.W. Influence of inherited geologic framework on barrier shoreface morphology and dynamics. *Mar. Geol.* **1995**, *126*, 213–234. [[CrossRef](#)]
18. Ashton, A.D.; Lorenzo-Trueba, J. Morphodynamics of barrier response to sea-level rise. In *Barrier Dynamics and Response to Changing Climate*; Moore, L.J., Murray, A.B., Eds.; Springer: Cham, Germany, 2018; pp. 277–304.
19. Shawler, J.L.; Ciarletta, D.J.; Connell, J.E.; Boggs, B.Q.; Lorenzo-Trueba, J.; Hein, C.J. Relative influence of antecedent topography and sea-level rise on barrier-island migration. *Sedimentology* **2021**, *68*, 639–669. [[CrossRef](#)]
20. Ortiz, A.C.; Ashton, A.D. Exploring shoreface dynamics and a mechanistic explanation for a morphodynamic depth of closure. *J. Geophys. Res. Earth Surf.* **2016**, *121*, 442–464. [[CrossRef](#)]
21. Rogers, L.J.; Moore, L.J.; Goldstein, E.B.; Hein, C.J.; Lorenzo-Trueba, J.; Ashton, A.D. Anthropogenic controls on overwash deposition: Evidence and consequences. *J. Geophys. Res. Earth Surf.* **2015**, *120*, 2609–2624. [[CrossRef](#)]
22. Miselis, J.L.; Lorenzo-Trueba, J. Natural and human-induced variability in barrier-island response to sea level rise. *Geophys. Res. Lett.* **2017**, *44*, 11–922. [[CrossRef](#)]
23. Thieler, E.; Brill, A.L.; Cleary, W.J.; Hobbs, C.H.; Gammisch, R.A. Geology of the Wrightsville Beach, North Carolina shoreface: Implications for the concept of shoreface profile of equilibrium. *Mar. Geol.* **1995**, *126*, 271–287. [[CrossRef](#)]

24. Wallace, D.J.; Anderson, J.B.; Fernández, R.A. Transgressive ravinement versus depth of closure: A geological perspective from the upper Texas coast. *J. Coast. Res.* **2010**, *26*, 1057–1067. [[CrossRef](#)]
25. Wernette, P.; Houser, C.; Weymer, B.A.; Everett, M.E.; Bishop, M.P.; Reece, B. Influence of a spatially complex framework geology on barrier island geomorphology. *Mar. Geol.* **2018**, *398*, 151–162. [[CrossRef](#)]
26. Bitencourt, V.J.; Dillenburg, S.R. Application of multivariate statistical techniques in alongshore differentiation of coastal barriers. *Mar. Geol.* **2020**, *419*, 106077. [[CrossRef](#)]
27. Demarest, J.M.; Leatherman, S.P. Mainland influence on coastal transgression: Delmarva Peninsula. *Mar. Geol.* **1985**, *63*, 19–33. [[CrossRef](#)]
28. Browder, A.G.; McNinch, J.E. Linking framework geology and nearshore morphology: Correlation of paleo-channels with shore-oblique sandbars and gravel outcrops. *Mar. Geol.* **2006**, *231*, 141–162. [[CrossRef](#)]
29. Honeycutt, M.G.; Krantz, D.E. Influence of the geologic framework on spatial variability in long-term shoreline change, Cape Henlopen to Rehoboth Beach, Delaware. *J. Coast. Res.* **2003**, 147–167. Available online: <https://www.jstor.org/stable/25736604> (accessed on 22 October 2020).
30. Pilkey, O.H.; Young, R.S.; Riggs, S.R.; Smith, A.S.; Wu, H.; Pilkey, W.D. The concept of shoreface profile of equilibrium: A critical review. *J. Coast. Res.* **1993**, *9*, 255–278.
31. Houser, C.; Hapke, C.; Hamilton, S. Controls on coastal dune morphology, shoreline erosion and barrier island response to extreme storms. *Geomorphology* **2008**, *100*, 223–240. [[CrossRef](#)]
32. Taney, N.E. *Geomorphology of the South Shore of Long Island, New York*; US Beach Erosion Board: Washington, DC, USA, 1961; No. 128.
33. Stone, B.D.; Borns, H.W., Jr. Pleistocene glacial and interglacial stratigraphy of New England, Long Island, and adjacent Georges Bank and Gulf of Maine. *Quat. Sci. Rev.* **1986**, *5*, 39–52. [[CrossRef](#)]
34. Williams, S.J. *Geomorphology, Shallow Subbottom Structure and Sediments of the Atlantic Inner-Continental Shelf off Long Island, New York*; Technical Paper No. 76-2; U.S. Army Corps of Engineers, Ed.; CERC: Fort Belvoir, VA, USA, 1976; p. 123.
35. Williams, S.J.; Duane, D.B. *Geomorphology and Sediments of the Inner New York Bight Continental Shelf*; TM-45; U.S. Army Corps of Engineers, Coastal Engineering Research Center: Fort Belvoir, VA, USA, 1974; p. 74.
36. Thompson, H.D. Hudson gorge in the Highlands. *Geol. Soc. Am. Bull.* **1936**, *47*, 1831–1848. [[CrossRef](#)]
37. Soren, J. *Results of Subsurface Exploration in the Mid-Island Area of Western Suffolk County, Long Island, New York*; No. LIWR-1; Suffolk County Water Authority: Oakdale, NY, USA, 1971.
38. Schwab, W.C.; Allison, M.A. Initial results of high-resolution seafloor mapping offshore of the New York–New Jersey metropolitan area using sidescan-sonar. *Northeast. Geol. Environ. Sci.* **1997**, *19*, 243–262.
39. Foster, D.S.; Swift, B.A.; Schwab, W.C. *Stratigraphic Framework Maps of the Nearshore Area of Southern Long Island from Fire Island to Montauk Point, New York*; U.S. Geological Survey Open-File Report; USGS: Woods Hole, MA, USA, 1999; pp. 99–559. Available online: <http://pubs.usgs.gov/of/1999/of99-559/> (accessed on 22 October 2020).
40. Newman, W.S.; Thurber, D.H.; Zeiss, H.S.; Rokach, A.; Musich, L. Late Quaternary geology of the Hudson River estuary: A preliminary report. *N. Y. Acad. Sci. Trans.* **1969**, *31*, 548–570. [[CrossRef](#)]
41. Uchupi, E.; Driscoll, N.; Ballard, R.; Bolmer, S. Drainage of late Wisconsin glacial lakes and the morphology and late quaternary stratigraphy of the New Jersey–southern New England continental shelf and slope. *Mar. Geol.* **2001**, *172*, 117–145. [[CrossRef](#)]
42. Sanderson, E.W. Cartographic evidence for historical geomorphological change and wetland formation in Jamaica Bay, New York. *Northeast. Nat.* **2016**, *23*, 277–304. [[CrossRef](#)]
43. USACE. *Atlantic Coast of New York, East Rockaway Inlet to Rockaway Inlet and Jamaica Bay: Draft Integrated Hurricane Sandy General Reevaluation Report and Environmental Impact Statement*; Final Report; USACE: Washington, DC, USA, 2016.
44. USACE. *Integrated Hurricane Sandy General Reevaluation Report and Environmental Impact Statement, Atlantic Coast of New York, East Rockaway Inlet to Rockaway Inlet and Jamaica Bay*; Final Report; USACE: Washington, DC, USA, 2019.
45. Hapke, C.J.; Lentz, E.E. A review of sediment budget imbalances along Fire Island, New York—Can nearshore geologic framework and patterns of shoreline change explain the deficit? *J. Coast. Res.* **2010**, *26*, 510–522. [[CrossRef](#)]
46. USACE. *Integrated Hurricane Sandy General Reevaluation Report and Environmental Impact Statement, Atlantic Coast of New York, East Rockaway Inlet to Rockaway Inlet and Jamaica Bay: Appendix A1 Shorefront Engineering and Design Appendix*; USACE: Washington, DC, USA, 2018.
47. Brutsché, K.E.; Rosati, J.; Pollock, C.E.; McFall, B.C. *Calculating Depth of Closure Using WIS Hindcast Data*; No. ERDC/CHL CHETN-VI-45; US Army Engineer Research and Development Center Vicksburg United States: Vicksburg, MI, USA, 2016.
48. Stalk, C.A.; DeWitt, N. *Coastal Bathymetry and Backscatter Data Collected in September and October 2019 from Rockaway Peninsula, New York*; U.S. Geological Survey Data Release; USGS: St. Petersburg, FL, USA, 2020. [[CrossRef](#)]
49. Forde, A.S.; Wei, E.A.; DeWitt, N.T.; Miselis, J.L. *Archive of Chirp Subbottom Profile Data Collected in 2019 from Rockaway Peninsula, New York*; U.S. Geological Survey Data Release; USGS: St. Petersburg, FL, USA, 2021. [[CrossRef](#)]
50. Cohen, J.K.; Stockwell, J.W., Jr. CWP/SU–Seismic Un*x Release No. 44—An Open Source Software Package for Seismic Research and Processing: Golden, Colo., Center for Wave Phenomena, Colorado School of Mines Web Page. 2020. Available online: <https://github.com/JohnWStockwellJr/SeisUnix> (accessed on 30 November 2010).

51. Mitchum, R.M., Jr.; Vail, P.R.; Sangree, J.B. *Seismic Stratigraphy and Global Changes of Sea Level, Part 6: Stratigraphic Interpretation of Seismic Reflection Patterns in Depositional Sequences: Section 2. Application of Seismic Reflection Configuration to Stratigraphic Interpretation*; AAPG: Tulsa, OK, USA, 1977.
52. Christie-Blick, N.; Driscoll, N.W. Sequence stratigraphy. *Annu. Rev. Earth Planet. Sci.* **1995**, *23*, 451–478. [[CrossRef](#)]
53. Locker, S.D.; Miselis, J.L.; Buster, N.L.; Hapke, C.J.; Wadman, H.M.; McNinch, J.E.; Forde, A.S.; Stalk, C.A. *Nearshore Sediment Thickness, Fire Island, New York*; US Geological Survey Open-File Report, No. 2017–1024; USGS: St. Petersburg, FL, USA, 2017; pp. 1–21. Available online: <https://pubs.er.usgs.gov/publication/ofr20171024/> (accessed on 31 August 2020).
54. Everhart, C.S.; Wei, E.A.; Miselis, J.L. *Grain-Size Data from Seven Mile Island, New Jersey and Rockaway Peninsula, New York*; U.S. Geological Survey Data Release; USGS: St. Petersburg, FL, USA, 2022. [[CrossRef](#)]
55. Cacchione, D.A.; Drake, D.E.; Grant, W.D.; Tate, G.B. Rippled scour depressions on the inner continental shelf off central California. *J. Sed. Res.* **1984**, *54*, 1280–1291.
56. Thieler, E.R.; Pilkey, O.H., Jr.; Cleary, W.J.; Schwab, W.C. Modern sedimentation on the shoreface and inner continental shelf at Wrightsville Beach, North Carolina, USA. *J. Sed. Res.* **2001**, *71*, 958–970. [[CrossRef](#)]
57. Murray, A.B.; Thieler, E.R. A new hypothesis and exploratory model for the formation of large-scale inner-shelf sediment sorting and “rippled scour depressions”. *Cont. Shelf Res.* **2004**, *24*, 295–315. [[CrossRef](#)]
58. Wei, E.A.; Miselis, J.L.; Forde, A.S. *Shoreface and Holocene Sediment Thickness Offshore of Rockaway Peninsula, New York*; U.S. Geological Survey Open-File Report 2021–1100; USGS: St. Petersburg, FL, USA, 2021. [[CrossRef](#)]
59. Rodriguez, A.B.; Fassell, M.L.; Anderson, J.B. Variations in shoreface progradation and ravinement along the Texas coast, Gulf of Mexico. *Sedimentology* **2001**, *48*, 837–853. [[CrossRef](#)]
60. Hallermeier, R.J. A profile zonation for seasonal sand beaches from wave climate. *Coast. Eng.* **1981**, *4*, 253–277. [[CrossRef](#)]
61. Schwab, W.C.; Thieler, E.R.; Allen, J.R.; Foster, D.S.; Swift, B.A.; Denny, J.F. Influence of inner-continental shelf geologic framework on the evolution and behavior of the barrier-island system between Fire Island Inlet and Shinnecock Inlet, Long Island, New York. *J. Coast. Res.* **2000**, *16*, 408–422.
62. Thieler, E.R.; Foster, D.S.; Himmelstoss, E.A.; Mallinson, D.J. Geologic framework of the northern North Carolina, USA inner continental shelf and its influence on coastal evolution. *Mar. Geol.* **2014**, *348*, 113–130. [[CrossRef](#)]
63. Mallinson, D.; Culver, S.; Leorri, E.; Mitra, S.; Mulligan, R.; Riggs, S. Barrier Island and estuary co-evolution in response to Holocene climate and sea-level change: Pamlico Sound and the Outer Banks Barrier Islands, North Carolina, USA. In *Barrier Dynamics and Response to Changing Climate*; Moore, L.J., Murray, A.B., Eds.; Springer: Cham, Germany, 2018; pp. 91–120.
64. Raff, J.L.; Shawler, J.L.; Ciarletta, D.J.; Hein, E.A.; Lorenzo-Trueba, J.; Hein, C.J. Insights into barrier-island stability derived from transgressive/regressive state changes of Parramore Island, Virginia. *Mar. Geol.* **2018**, *403*, 1–19. [[CrossRef](#)]
65. NOAA Office of Coast Survey. Historical Map and Chart Collection. 2020. Available online: <https://historicalcharts.noaa.gov/> (accessed on 4 March 2020).
66. Liu, S.; Goff, J.A. Lower shoreface seismic stratigraphy and morphology off Fire Island, New York: Evidence for lobate progradation and linear erosion. *Cont. Shelf Res.* **2018**, *163*, 23–34. [[CrossRef](#)]
67. Coch, N.K. Forensic Analysis of the 1893 “New York City” Hurricane: Implications for the Future. *J. Coast. Res.* **2019**, *35*, 729–736. [[CrossRef](#)]
68. Cattaneo, A.; Steel, R.J. Transgressive deposits: A review of their variability. *Earth-Sci. Rev.* **2003**, *62*, 187–228. [[CrossRef](#)]
69. Backstrom, J.; Jackson, D.; Cooper, J. Shoreface morphodynamics of a high-energy, steep and geologically constrained shoreline segment in Northern Ireland. *Mar. Geol.* **2009**, *257*, 94–106. [[CrossRef](#)]
70. Cooper, J.; Kelley, J.; Belknap, D.; Quinn, R.; McKenna, J. Inner shelf seismic stratigraphy off the north coast of Northern Ireland: New data on the depth of the Holocene lowstand. *Mar. Geol.* **2002**, *186*, 369–387. [[CrossRef](#)]
71. Siringan, F.P.; Anderson, J.B. Modern shoreface and inner-shelf storm deposits off the east Texas coast, Gulf of Mexico. *J. Sed. Res.* **1994**, *64*, 99–110.
72. Cooper, J.; Green, A.; Loureiro, C. Geological constraints on mesoscale coastal barrier behaviour. *Glob. Planet Chang.* **2018**, *168*, 15–34. [[CrossRef](#)]
73. Anthony, E.J.; Aagaard, T. The lower shoreface: Morphodynamics and sediment connectivity with the upper shoreface and beach. *Earth Sci. Rev.* **2020**, *210*, 103334. [[CrossRef](#)]
74. Goff, J.A. Seismic and core investigation off Panama city, Florida, reveals sand ridge influence on formation of the shoreface ravinement. *Cont. Shelf Res.* **2014**, *88*, 34–46. [[CrossRef](#)]
75. Oakley, B.A.; Murphy, C.; Varney, M.; Hollis, R.J. Spatial extent and volume of the shoreface depositional platform on the upper shoreface of the glaciated Rhode Island south shore. *Estuaries Coast.* **2019**, *45*, 1123–1142. [[CrossRef](#)]
76. Goff, J.A.; Flood, R.D.; Austin, J.J.A.; Schwab, W.C.; Christensen, B.; Browne, C.M.; Denny, J.F.; Baldwin, W.E. The impact of Hurricane Sandy on the shoreface and inner shelf of Fire Island, New York: Large bedform migration but limited erosion. *Cont. Shelf Res.* **2015**, *98*, 13–25. [[CrossRef](#)]
77. Rodriguez, A.B.; Anderson, J.B.; Bradford, J. Holocene Tidal Deltas of the Trinity Incised Valley: Analogs for Exploration and Production. *Gulf. Coast. Assoc. Geol. Soc. Trans.* **1998**, *48*, 373–380.
78. Driscoll, N.W.; Karner, G.D. Three dimensional quantitative modeling of clinof orm development. *Mar. Geol.* **1999**, *154*, 383–398. [[CrossRef](#)]

79. Hequette, A.; Desrosiers, M.; Hill, P.R.; Forbes, D.L. The influence of coastal morphology on shoreface sediment transport under storm-combined flows, Canadian Beaufort Sea. *J. Coast. Res.* **2001**, *17*, 507–516.
80. Aagaard, T.; Hughes, M.G. Equilibrium shoreface profiles: A sediment transport approach. *Mar. Geol.* **2017**, *390*, 321–330. [[CrossRef](#)]
81. Cowell, P.; Roy, P.; Jones, R. Simulation of large-scale coastal change using a morphological behaviour model. *Mar. Geol.* **1995**, *126*, 45–61. [[CrossRef](#)]
82. Robertson, W.; Zhang, K.; Finkl, C.W.; Whitman, D. Hydrodynamic and geologic influence of event-dependent depth of closure along the South Florida Atlantic Coast. *Mar. Geol.* **2008**, *252*, 156–165. [[CrossRef](#)]
83. Jackson, D.W.T.; Cooper, J.A.G. Geological control on beach form: Accommodation space and contemporary dynamics. *J. Coast. Res.* **2009**, *56*, 69–72.